

# Sequential Detection and Estimation of Multipath Channel Parameters Using Belief Propagation

Xuhong Li<sup>†</sup>, *Student Member, IEEE*, Erik Leitinger<sup>†</sup>, *Member, IEEE*,  
Alexander Venus, *Student Member, IEEE*, and Fredrik Tufvesson, *Fellow, IEEE*

<sup>†</sup> Have equally contributed as first authors.

**Abstract**—This paper proposes a belief propagation (BP)-based algorithm for sequential detection and estimation of multipath component (MPC) parameters based on radio signals. Under dynamic channel conditions with moving transmitter/receiver, the number of MPCs, the MPC dispersion parameters, and the number of false alarm contributions are unknown and time-varying. We develop a Bayesian model for sequential detection and estimation of MPC dispersion parameters, and represent it by a factor graph enabling the use of BP for efficient computation of the marginal posterior distributions. At each time step, a snapshot-based parametric channel estimator provides parameter estimates of a set of MPCs which are used as noisy measurements by the proposed BP-based algorithm. It performs joint probabilistic data association, and estimation of the time-varying MPC parameters and the mean number of false alarm measurements, by means of the sum-product algorithm rules. The algorithm also exploits amplitude information enabling the reliable detection of “weak” MPCs with very low component signal-to-noise ratios (SNRs). The performance of the proposed algorithm compares well to state-of-the-art algorithms for high SNR MPCs, but it significantly outperforms them for medium or low SNR MPCs. Results using real radio measurements demonstrate the excellent performance of the proposed algorithm in realistic and challenging scenarios.

**Index Terms**—Multipath channel, parametric channel estimation, data association, factor graphs, belief propagation, sum-product algorithm.

## I. INTRODUCTION

The information of dispersive wireless radio channels and its temporal behavior in dynamic scenarios are of great importance for the development of radio channel models [1], [2], 5G

Xuhong Li and Fredrik Tufvesson are with the Department of Electrical and Information Technology, Lund University, 221 00 Lund, Sweden (e-mail: {xuhong.li, fredrik.tufvesson}@eit.lth.se). Erik Leitinger and Alexander Venus are with the Laboratory of Signal Processing and Speech Communication and the Christian Doppler Laboratory for Location-aware Electronic Systems, Graz University of Technology, 8010 Graz, Austria (e-mail: {erik.leitinger, a.venus}@tugraz.at).

This work was supported in part by the Swedish Research Council (VR), in part by the strategic research area Excellence Center at Linköping—Lund in Information Technology (ELLIIT), in part by the Christian Doppler Research Association and in part by the TU Graz.

This article was presented in part at the 54th IEEE Asilomar Conference on Signals, Systems, and Computers, Pacific Grove, CA, USA, October 2020 (DOI: 10.1109/IEEECONF51394.2020.9443465). This article is accepted for publication in IEEE Transactions on Wireless Communications, 2022 (DOI:10.1109/TWC.2022.3165856). Compared to the IEEE version, this arXiv version provides additional simulation results in Appendix E.

wireless communication technologies [3]–[5], and multipath-based localization and mapping [6]–[10]. The response of a non-static wireless radio channel is typically represented by superimposed weighted Dirac delta distributions with distinct and time-varying locations (or supports) in the respective dispersion domains (delay, angle-of-arrival (AoA), angle-of-departure, Doppler frequency, and combinations thereof). Each component is meant to represent a multipath component (MPC). In general, the channel response can be observed only within a finite aperture leading to some limitations on the ability to resolve MPCs closely spaced in the dispersion domains. The related time-varying MPC parameters are usually estimated from multi-dimensional measurements using antenna arrays and multiple frequencies (wideband or ultra-wideband (UWB)) [11] using super-resolution (SR) algorithms that perform sequential estimation of MPC parameters.

### A. State-of-the-Art Methods

If the number-of-MPCs (NoM) is known, subspace methods [12]–[14] or maximum likelihood (ML) methods as for example [15] are standard SR methods to estimate time-invariant MPC parameters. Expectation maximization-based methods [16], have been proven a viable approximation of the computationally prohibitive ML methods [17]. In recent years, a channel model has been introduced that also considers dense multipath components (DMC) [18]. The DMC incorporates MPCs that cannot be resolved due to finite observation aperture. Including the estimation of DMC can improve the accuracy of the parameter estimation of distinct MPCs.

All afore mentioned methods have in common that they do not incorporate the estimation of the NoM into the estimation problem. One classical solution is to extend the methods with an outer stage for NoM detection using for example eigenvalue-based methods, or the generic information theoretic criteria, e.g., the Akaike/Bayesian information criterion, the minimum description length (MDL) principle [19]. The outer stage schemes mostly tend to overestimate the NoM. Inspired by the ideas of sparse estimation and compressed sensing, some SR sparse Bayesian parametric channel estimation algorithms [11], [20]–[22] have recently appeared which aim to reconstruct sparse signals from a reduced set of measurements specified by a sparse weight vector. By introducing a sparsity-promoting prior model for the weights, the estimation of the

NoM and MPC parameters can be jointly formulated in a Bayesian framework.

To capture the temporal behaviors of MPC parameters in time-varying scenarios, many sequential estimation methods have been proposed, which can be grouped into two broad categories. Methods of the first category sequentially estimate the MPC parameters directly based on the radio signals using for example an extended Kalman filter [23]–[26]. Methods of the second category adopt a two-stage structure where the estimates of a snapshot-based channel estimator are used as measurements in a tracking filter [27]. In this work, we focus on the two-stage methods. Due to the finite aperture of measurement systems and the resolution capability of snapshot-based parametric channel estimators, some measurements might not be well resolved hence incorporate contributions from more than one MPCs and false alarms may exist. In this case, to decide which measurement should be used for the update of which MPC (i.e., data association (DA) problem) can be complicated. In general, existing sequential channel estimation methods adopt “hard” association which assumes that measurements are fine resolved and each of them originates from single MPC that is specified by metrics such as the global nearest neighbor [28]. Probabilistic DA [28], [29], on the other hand, solves the origin uncertainty problem in a “soft” manner, in which the association probabilities for all current measurements are computed and used to form a mixture probability density function (PDF) for the update of each MPC state.

### B. Contributions

Here, we propose a belief propagation (BP)-based algorithm for sequential detection of MPCs and estimation of their dispersion parameters that uses the MPC estimates from a snapshot-based parametric SR-sparse Bayesian learning (SBL) channel estimator (abbreviated as SR-SBL) as measurements [11], [21], [22], [30].<sup>1</sup> To reduce the computational demand and to improve the convergence behavior of the snapshot-based estimator, statistical information of the dispersion parameters of the BP-based algorithm is fed back to the SR-SBL channel estimator. The proposed algorithm jointly performs probabilistic DA and sequential estimation of potential MPC (PMPC) parameters by running the BP-based algorithm, also known as the sum-product algorithm, on a factor graph [8], [29], [33], [34]. Note that independence between MPCs is assumed throughout the work. We use a probabilistic model for MPC existence where each PMPC state is augmented by a binary existence variable and associated with an existence probability, which is also estimated and used for the detection of reliable MPCs modeling the birth and death of these components [8], [35]. The complex amplitudes of MPCs are an integral part of the multipath channel model and must be estimated

<sup>1</sup>This work is inspired by the BP-based SLAM algorithm presented in [8], [31], [32]. The main novelties of the proposed algorithm over the previous work are threefold: (i) we present more detailed derivations for the joint prior PDFs and joint likelihoods; (ii) we extend the prior work with adaptive estimation of the mean number of false alarms (MNFA); (iii) we apply the prior work successfully to the field of parametric radio channel estimation.

alongside with the dispersion parameters. Therefore, they are incorporated into the proposed algorithm. More specifically, the algorithm uses the statistics of MPC amplitudes to determine the unknown and time-varying detection probabilities [31], [32], [36], [37], which improves the detectability and maintenance of low signal-to-noise ratio (SNR) MPCs, and enables a better discrimination against false alarms. Knowing the correct mean number of false alarms (MNFA) is crucial for optimal performance of Bayesian detection and estimation algorithms. However, determining the MNFA in advance is not straightforward, especially, if the MNFA is time-varying. Using a fixed predefined value of MNFA that deviates largely from the true one, can potentially lead to decreased detection performance of MPCs and an increased number of detected false alarms. The proposed algorithm estimates the possibly time-varying MNFA to cope with false alarm measurements originating from the preprocessing step and clutter measurements originating from strongly fluctuating scattered MPCs (as for example DMC). The main contributions of this paper are summarized as follows.

- We introduce a Bayesian model for sequential detection and estimation of MPC parameters, which uses the estimates from a snapshot-based channel estimator as measurements. Within this model, the death and birth of MPCs and DAs are formulated probabilistically, and adaptive detection probabilities are incorporated by exploiting amplitude information.
- We further present a BP-based algorithm based on the factor graph representation of the estimation problem, where the PMPC states and the MNFA are estimated jointly and sequentially.
- The performance of the proposed algorithm is demonstrated with both synthetic and real measurements. Moreover, the results are compared with the Kalman enhanced super resolution tracking (KEST) [27] algorithm (a state-of-the-art sequential parametric channel estimation method), and posterior Cramér–Rao lower bound (CRLB) (PCRLB).

This paper advances over our preliminary conference publication [38] by (i) presenting a detailed derivations of the factor graph, (ii) including the detailed derivations of the factors related to the MNFA, (iii) establishing a particle-based implementation of the proposed algorithm, (iv) validating the performance with additional simulated and real scenarios, and (v) demonstrating a comparison with a state-of-the-art method and the PCRLB.

*Notations:* Column vectors and matrices are denoted by boldface lowercase and uppercase letters. Random variables are displayed in san serif, upright fonts as for example  $x$  and  $\mathbf{x}$  and their realizations in serif, italic font as for example  $x$  and  $\mathbf{x}$ .  $f(\mathbf{x})$  denotes the PDF or probability mass function (PMF) of continuous or discrete random vector.  $(\cdot)^T$ ,  $(\cdot)^*$ , and  $(\cdot)^H$  denote matrix transpose, complex conjugation and Hermitian transpose, respectively.  $\|\cdot\|$  is the Euclidean norm.  $|\cdot|$  represents the cardinality of a set.  $\text{diag}\{\mathbf{x}\}$  denotes a

diagonal matrix with entries in  $\mathbf{x}$ .  $\text{tr}\{\cdot\}$  denotes the trace of a matrix.  $\mathbf{I}_{[\cdot]}$  is an identity matrix of dimension given in the subscript.  $[\mathbf{X}]_{n,n}$  denotes the  $n$ th diagonal entry of  $\mathbf{X}$ .  $[\mathbf{X}]_{1:n}$  denotes a sub-matrix containing  $1:n$  columns and rows of  $\mathbf{X}$ . Furthermore,  $\bar{1}(e)$  denotes the function of the event  $e = 0$  (i.e.,  $\bar{1}(e) = 1$  if  $e = 0$  and 0 otherwise).  $1_{\mathbb{A}}(\mathbf{x})$  denotes the indicator function that is  $1_{\mathbb{A}}(\mathbf{x}) = 1$  if  $\mathbf{x} \in \mathbb{A}$  and 0 otherwise. For any function  $g(\mathbf{x})$  we define the integral  $\langle g(\mathbf{x}) \rangle_{f(\mathbf{x})} = \int g(\mathbf{x})f(\mathbf{x})d\mathbf{x}$ . As for example  $\langle \mathbf{x} \rangle_{f(\mathbf{x})} = \int \mathbf{x}f(\mathbf{x})d\mathbf{x}$  and  $\langle f(\mathbf{x}) \rangle_{1_{\mathbb{A}}(\mathbf{x})} = \int_{\mathbb{A}} f(\mathbf{x})d\mathbf{x}$  denote the expected value and the integral over  $f(\mathbf{x})$  of the random vector  $\mathbf{x}$ , respectively.

## II. RADIO SIGNAL MODEL

We consider a single-input multiple-output (SIMO) UWB system, where the transmitter (Tx) uses a single antenna, and the receiver (Rx) is equipped with an antenna array made of  $H$  elements located at  $\mathbf{p}_n^{(h)} \in \mathbb{R}^{2 \times 1}$  with  $h \in \{1, \dots, H\}$ .<sup>2</sup> We define  $d_n^{(h)} = \|\mathbf{p}_n^{(h)} - \mathbf{p}_n\|$  and  $\varphi_n^{(h)} = \angle(\mathbf{p}_n^{(h)} - \mathbf{p}_n) - \psi$ , as the distance of the  $h$ th element to the reference location  $\mathbf{p}_n \in \mathbb{R}^{2 \times 1}$ , i.e., the array's center of gravity, and its angle relative to the array orientation  $\psi$ , respectively. For the sake of brevity, we assume a two-dimensional scenario with horizontal-only propagation.<sup>3</sup>

### A. Received Signal

Signals are represented by their complex envelopes with respect to a center frequency  $f_c$ . The single antenna at the transmitter emits a periodic signal  $\tilde{s}(t)$ . The received signal at each antenna element  $h$  at the discrete observation time  $n$  is given as [11], [18], [39]

$$s_{\text{RX},n}^{(h)}(t) = \sum_{l=1}^{L_n} \tilde{\alpha}_{l,n} s(t; \tilde{d}_{l,n}, \tilde{\varphi}_{l,n}, \mathbf{p}_n^{(h)}) + \omega_n^{(h)}(t) \quad (1)$$

where the first term comprises  $L_n$  MPCs, with each being characterized by its complex amplitude  $\tilde{\alpha}_{l,n} \in \mathbb{C}$ , distance  $\tilde{d}_{l,n} = c\tilde{\tau}_{l,n} \in \mathbb{R}$  to the array's center of gravity directly related to the time delay via the speed of light  $c$ , and AoA  $\tilde{\varphi}_{l,n} \in [-\pi, \pi)$  w.r.t. the array orientation. Under the far-field plane-wave assumption, the signal  $s(t; \tilde{d}, \tilde{\varphi}, \mathbf{p}^{(h)})$  is given as  $s(t; \tilde{d}, \tilde{\varphi}, \mathbf{p}^{(h)}) = e^{j2\pi f_c g(\tilde{\varphi}, \mathbf{p}^{(h)})} \tilde{s}(t - \tilde{d}/c + g(\tilde{\varphi}, \mathbf{p}^{(h)}))$ . The function  $g(\tilde{\varphi}, \mathbf{p}^{(h)}) = \frac{d^{(h)} \cos(\tilde{\varphi} - \psi - \varphi^{(h)})}{c}$  gives the delay shift of a plane-wave incident with AoA  $\tilde{\varphi}$  being measured relatively to the array orientation  $\psi$ , at the  $h$ th antenna position w.r.t. the array's center of gravity. We assume that the Tx and Rx are time synchronized and the array orientation is known. The measurement noise process  $\omega_n^{(h)}(t)$  in (1) is independent additive white Gaussian noise (AWGN) with double-sided power spectral density  $N_0/2$ .

<sup>2</sup>Note that the extension of the algorithm to a multiple-input single-output (MISO) or a multiple-input multiple-output (MIMO) system considering an antenna array at the Tx is straightforward.

<sup>3</sup>An extension to three-dimensional scenarios with horizontal and vertical propagation is straightforward, but it would lead to a cumbersome notation and one would not gain any further insights.

The received signal in (1) observed over a duration  $T$  is sampled with frequency  $f_s = 1/T_s$  at each time  $n$ , yielding a length  $N_s = T/T_s$  sample vector  $\mathbf{s}_{\text{RX},n}^{(h)} \in \mathbb{C}^{N_s \times 1}$  from each array element. By stacking  $\mathbf{s}_{\text{RX},n}^{(h)}$  from  $H$  array elements, the discrete time signal vector  $\mathbf{s}_{\text{RX},n} \triangleq [\mathbf{s}_{\text{RX},n}^{(1)\text{T}} \cdots \mathbf{s}_{\text{RX},n}^{(H)\text{T}}]^\text{T} \in \mathbb{C}^{N_s H \times 1}$  is given by

$$\mathbf{s}_{\text{RX},n} = \mathbf{S}(\tilde{\boldsymbol{\theta}}_n) \tilde{\boldsymbol{\alpha}}_n + \boldsymbol{\omega}_n. \quad (2)$$

In the first summand  $\tilde{\boldsymbol{\alpha}}_n \triangleq [\tilde{\alpha}_{1,n} \cdots \tilde{\alpha}_{L_n,n}]^\text{T} \in \mathbb{C}^{L_n \times 1}$ ,  $\tilde{\boldsymbol{\theta}}_n \triangleq [\tilde{\boldsymbol{\theta}}_{1,n}^\text{T} \cdots \tilde{\boldsymbol{\theta}}_{L_n,n}^\text{T}]^\text{T} \in \mathbb{R}^{2L_n \times 1}$  with  $\tilde{\boldsymbol{\theta}}_{l,n} \triangleq [\tilde{d}_{l,n} \tilde{\varphi}_{l,n}]^\text{T} \in \mathbb{R}^{2 \times 1}$  denoting the vector comprising the MPC parameters, and  $\mathbf{S}(\tilde{\boldsymbol{\theta}}_n) \triangleq [\mathbf{s}(\tilde{\boldsymbol{\theta}}_{1,n}) \cdots \mathbf{s}(\tilde{\boldsymbol{\theta}}_{L_n,n})] \in \mathbb{C}^{N_s H \times L_n}$  with columns given by  $\mathbf{s}(\tilde{\boldsymbol{\theta}}_{l,n}) = [\mathbf{s}_1(\tilde{\boldsymbol{\theta}}_{l,n})^\text{T} \cdots \mathbf{s}_H(\tilde{\boldsymbol{\theta}}_{l,n})^\text{T}]^\text{T} \in \mathbb{C}^{N_s H \times 1}$ . The  $h$ th entry of  $\mathbf{s}(\tilde{\boldsymbol{\theta}}_{l,n})$  reads  $s_h(\tilde{\boldsymbol{\theta}}_{l,n}) \triangleq [s(-[(N-1)/2]T_s; \tilde{d}_{l,n}, \tilde{\varphi}_{l,n}, \mathbf{p}^{(h)}) \cdots s([(N-1)/2]T_s; \tilde{d}_{l,n}, \tilde{\varphi}_{l,n}, \mathbf{p}^{(h)})]^\text{T} \in \mathbb{C}^{N_s \times 1}$ . The measurement noise vector  $\boldsymbol{\omega}_n \in \mathbb{C}^{N_s H \times 1}$  is a complex circularly symmetric Gaussian random vector with covariance matrix  $\mathbf{C} = \sigma^2 \mathbf{I}_{N_s H}$ , where  $\sigma^2 = N_0/T_s$  is the noise variance. The component SNR of each MPC is  $\widetilde{\text{SNR}}_{l,n} = \frac{|\tilde{\alpha}_{l,n}|^2 \|\mathbf{s}(\tilde{\boldsymbol{\theta}}_{l,n})\|^2}{\sigma^2}$  and the according normalized

amplitude equals  $\tilde{u}_{l,n} = \sqrt{\widetilde{\text{SNR}}_{l,n}}$ . An MPC exists only when its associated geometric feature is visible at the Rx position. The true number  $L_n$  of MPCs as well as their individual parameters  $\tilde{u}_{l,n}$ ,  $\tilde{d}_{l,n}$ , and  $\tilde{\varphi}_{l,n}$  are unknown and time-varying in dynamic scenarios. We propose an algorithm to sequentially detect and estimate these parameters.

### B. Parametric Channel Estimation

Based on the discrete time signal vector in (2), a snapshot-based SR-SBL estimator [11], [20]–[22], [30] provides estimated dispersion parameters of  $M_n$  multipath components (MPCs) stacked into the vector  $\mathbf{z}_n \triangleq [\mathbf{z}_{1,n}^\text{T} \cdots \mathbf{z}_{M_n,n}^\text{T}]^\text{T} \in \mathbb{R}^{3M_n \times 1}$  at each time  $n$ . An entry  $\mathbf{z}_{m,n} \triangleq [z_{d,m,n} \ z_{\varphi,m,n} \ z_{u,m,n}]^\text{T} \in \mathbb{R}^{3 \times 1}$  comprises the distance estimate  $z_{d,m,n}$ , the AoA estimate  $z_{\varphi,m,n}$ , and the normalized amplitude estimate  $z_{u,m,n}$  of an MPC. The normalized amplitude estimate is given by  $z_{u,m,n} \triangleq |\mu_{\alpha_{m,n}}|/\sigma_{\alpha_{m,n}}$  where  $\mu_{\alpha_{m,n}}$  and  $\sigma_{\alpha_{m,n}}$  denote, respectively, the estimated mean and standard deviation of the complex amplitudes. Note that all estimated component SNRs given by  $z_{u,m,n}^2$  are above a predefined detection threshold  $u_{\text{de}}$ . The estimated amplitudes  $z_{u,m,n}$  are directly related to the detection probabilities of the corresponding MPCs [31], [32] (see Section III-C). At time  $n = 1$ , the initial prior PDF of the dispersion parameters considered in the snapshot-based estimator is uniform over the validation region. For each time  $n \geq 2$ , the snapshot-based estimator is initialized with  $\hat{L}_{n-1}$  detected MPCs returned from the BP-based algorithm at time  $n-1$  (see Section IV-B). The vector  $\mathbf{z}_n$  is used as noisy measurement by the proposed algorithm. Note that the snapshot-based estimator decomposes  $\mathbf{s}_{\text{RX},n}$  into individual, decorrelated components with parameters stacked into  $\mathbf{z}_n$ , reducing the number of dimensions (as  $M_n$  is usually much smaller than  $N_s H$ ).

### III. SYSTEM MODEL

#### A. PMPC States

Following [8], [29], we account for the time-varying and unknown NoM by introducing PMPCs indexed by  $k \in \{1, \dots, K_n\}$ . The number of PMPCs  $K_n$  is the maximum number of actual MPCs that have produced measurements so far [29]. The existence/non-existence of PMPC  $k$  as an actual MPC is modeled by a binary random variable  $r_{k,n} \in \mathbb{B} = \{0, 1\}$  in the sense that a PMPC exists if and only if  $r_{k,n} = 1$ . Augmented states of PMPCs are denoted as  $\mathbf{y}_{k,n} \triangleq [\mathbf{x}_{k,n}^T r_{k,n}]^T \in \mathbb{R}^{5 \times 1} \times \mathbb{B}$ , where  $\mathbf{x}_{k,n} = [\boldsymbol{\theta}_{k,n}^T u_{k,n} v_{d_{k,n}} v_{\varphi_{k,n}}]^T \in \mathbb{R}^{5 \times 1}$ ,  $\boldsymbol{\theta}_{k,n} = [d_{k,n} \varphi_{k,n}]^T \in \mathbb{R}^{2 \times 1}$ , and  $v_{d_{k,n}}$  and  $v_{\varphi_{k,n}}$  are the distance velocity and angular velocity, respectively.

Formally, PMPC  $k$  is also considered even if it is non-existent, i.e.,  $r_{k,n} = 0$ . The states  $\mathbf{x}_{k,n}$  of non-existent PMPCs are obviously irrelevant and have no influence on the PMPC detection and state estimation. Therefore, all PDFs defined for PMPC states,  $f(\mathbf{y}_{k,n}) = f(\mathbf{x}_{k,n}, r_{k,n})$ , are of the form  $f(\mathbf{x}_{k,n}, r_{k,n} = 0) = f_{k,n} f_D(\mathbf{x}_{k,n})$ , where  $f_D(\mathbf{x}_{k,n})$  is an arbitrary ‘‘dummy PDF’’ and  $f_{k,n} \in [0, 1]$  is a constant representing the probability of non-existence [8], [29], [35].

#### B. State-Transition Model

For each PMPC with state  $\mathbf{y}_{k,n-1}$  with  $k \in \{1, \dots, K_{n-1}\}$  at time  $n-1$ , there is one ‘‘legacy’’ PMPC with state  $\underline{\mathbf{y}}_{k,n} \triangleq [\underline{\mathbf{x}}_{k,n}^T r_{k,n}]^T$  with  $k \in \{1, \dots, K_{n-1}\}$  at time  $n$ . Assuming that PMPC states evolve independently across  $k$  and  $n$ , the corresponding state-transition PDF of the joint states  $\mathbf{y}_{n-1} \triangleq [\mathbf{y}_{1,n-1}^T \dots \mathbf{y}_{K_{n-1},n-1}^T]^T$  and  $\underline{\mathbf{y}}_n \triangleq [\underline{\mathbf{y}}_{1,n}^T \dots \underline{\mathbf{y}}_{K_{n-1},n}^T]^T$  factorizes as [29]

$$f(\underline{\mathbf{y}}_n | \mathbf{y}_{n-1}) = \prod_{k=1}^{K_{n-1}} f(\underline{\mathbf{y}}_{k,n} | \mathbf{y}_{k,n-1}) \quad (3)$$

where  $f(\underline{\mathbf{y}}_{k,n} | \mathbf{y}_{k,n-1}) = f(\underline{\mathbf{x}}_{k,n}, r_{k,n} | \mathbf{x}_{k,n-1}, r_{k,n-1})$  is the single PMPC state-transition PDF. If a PMPC did not exist at time  $n-1$ , i.e.,  $r_{k,n-1} = 0$ , it cannot exist at time  $n$  as a legacy PMPC. This means that

$$f(\underline{\mathbf{x}}_{k,n}, r_{k,n} | \mathbf{x}_{k,n-1}, 0) = \begin{cases} f_D(\underline{\mathbf{x}}_{k,n}), & r_{k,n} = 0 \\ 0, & r_{k,n} = 1. \end{cases} \quad (4)$$

If a PMPC existed at time  $n-1$ , i.e.,  $r_{k,n-1} = 1$ , at time  $n$  it either dies i.e.,  $r_{k,n} = 0$  or it still exists i.e.,  $r_{k,n} = 1$ , with the survival probability denoted as  $p_s$ . If it does survive, the state  $\underline{\mathbf{x}}_{k,n}$  is distributed according to the state-transition PDF  $f(\underline{\mathbf{x}}_{k,n} | \mathbf{x}_{k,n-1})$ . Thus,

$$f(\underline{\mathbf{x}}_{k,n}, r_{k,n} | \mathbf{x}_{k,n-1}, 1) = \begin{cases} (1 - p_s) f_D(\underline{\mathbf{x}}_{k,n}), & r_{k,n} = 0 \\ p_s f(\underline{\mathbf{x}}_{k,n} | \mathbf{x}_{k,n-1}), & r_{k,n} = 1. \end{cases} \quad (5)$$

We also define the state vector for all times up to  $n$  of legacy PMPCs as  $\underline{\mathbf{y}}_{1:n} \triangleq [\underline{\mathbf{y}}_1^T \dots \underline{\mathbf{y}}_n^T]^T$ .

#### C. Measurement Model

Before the current measurements  $\mathbf{z}_n$  are observed, the number of measurements  $M_n$  is a random variable. The vector collecting the number of measurements is defined as  $\mathbf{m}_{1:n} \triangleq [M_1 \dots M_n]^T$ . The conditional PDF  $f(\mathbf{z}_{m,n} | \mathbf{x}_{k,n})$  of  $\mathbf{z}_n$  assumes that the individual measurements  $\mathbf{z}_{m,n}$  are conditionally independent given the state  $\mathbf{x}_{k,n}$ . At each time  $n$ , a snapshot-based channel estimator provides the current observed measurement vector  $\mathbf{z}_n = [z_{1,n}^T \dots z_{M_n,n}^T]^T$  (see Section II), which is not random anymore and with fixed  $M_n$ . If  $\mathbf{z}_{m,n}$  is a PMPC-oriented measurement, we assume that the conditional PDF  $f(\mathbf{z}_{m,n} | \mathbf{x}_{k,n})$  is conditionally independent across  $z_{d_{m,n}}$ ,  $z_{\varphi_{m,n}}$ , and  $z_{u_{m,n}}$  given the states  $d_{k,n}$ ,  $\varphi_{k,n}$ , and  $u_{k,n}$ , thus it factorizes as

$$f(\mathbf{z}_{m,n} | \mathbf{x}_{k,n}) = f(z_{d_{m,n}} | d_{k,n}, u_{k,n}) f(z_{\varphi_{m,n}} | \varphi_{k,n}, u_{k,n}) \times f(z_{u_{m,n}} | u_{k,n}) \quad (6)$$

where the individual likelihood functions of the distance measurement  $f(z_{d_{m,n}} | d_{k,n}, u_{k,n})$  and the AoA measurement  $f(z_{\varphi_{m,n}} | \varphi_{k,n}, u_{k,n})$  are modeled by Gaussian PDFs, i.e.,

$$f(z_{d_{m,n}} | d_{k,n}, u_{k,n}) = (2\pi\sigma_{d_{k,n}}^2)^{-\frac{1}{2}} e^{-\frac{(z_{d_{m,n}} - d_{k,n})^2}{2\sigma_{d_{k,n}}^2}} \quad (7)$$

and

$$f(z_{\varphi_{m,n}} | \varphi_{k,n}, u_{k,n}) = (2\pi\sigma_{\varphi_{k,n}}^2)^{-\frac{1}{2}} e^{-\frac{(z_{\varphi_{m,n}} - \varphi_{k,n})^2}{2\sigma_{\varphi_{k,n}}^2}}. \quad (8)$$

The variances depend on  $u_{k,n}$  and are determined based on the Fisher information, respectively, given by  $\sigma_{d_{k,n}}^2 = c^2 / (8\pi^2 \beta_{\text{bw}}^2 u_{k,n}^2)$  and  $\sigma_{\varphi_{k,n}}^2 = c^2 / (8\pi^2 f_c^2 u_{k,n}^2 D^2(\varphi_{k,n}))$ , where the latter is a function of the PMPC state  $\varphi_{k,n}$  [32], [40]. Here,  $\beta_{\text{bw}}^2$  is the mean square bandwidth of the signal  $\tilde{s}(t)$  and  $D^2(\varphi_{k,n})$  is the squared array aperture. The likelihood function  $f(z_{u_{m,n}} | u_{k,n})$  of the normalized amplitude measurement  $z_{u_{m,n}}$  is modeled by a truncated Rician PDF [28, Ch. 1.6.7], i.e.,

$$f(z_{u_{m,n}} | u_{k,n}) = \frac{\frac{z_{u_{m,n}}}{\sigma_{u_{k,n}}} e^{\left(\frac{-z_{u_{m,n}}^2 + u_{k,n}^2}{2\sigma_{u_{k,n}}^2}\right)} I_0\left(\frac{z_{u_{m,n}} u_{k,n}}{\sigma_{u_{k,n}}^2}\right)}{p_d(u_{k,n})} \quad (9)$$

for  $z_{u_{m,n}} > \sqrt{u_{\text{de}}}$ , where the squared scale parameter  $\sigma_{u_{k,n}}^2$  depends on  $u_{k,n}$  and is determined based on the Fisher information given by  $\sigma_{u_{k,n}}^2 = \frac{1}{2} + \frac{1}{4N_s H} u_{k,n}^2$ ,  $I_0(\cdot)$  represents the 0th-order modified first-kind Bessel function, and  $u_{\text{de}}$  is the detection threshold of the snapshot-based estimator. The derivation of the squared scale parameter is given in Appendix D. The detection probability (i.e., the probability that a PMPC  $\mathbf{y}_{k,n}$  generates a measurement  $\mathbf{z}_{m,n}$ ) is modeled by a Rician cumulative distribution function (CDF), i.e.,  $p_d(u_{k,n}) = Q_1(u_{k,n} / \sigma_{u_{k,n}}, \sqrt{u_{\text{de}}} / \sigma_{u_{k,n}})$  [31], [32], [36], where the CDF  $Q_1(\cdot, \cdot)$  denotes the Marcum Q-function [28, Ch. 1.6.7]. Note that  $p_d(u_{k,n})$  is directly related to the MPC's visibility and the component SNR as well as to the snapshot-based estimator.

False alarm measurements originating from the snapshot-

based parametric channel estimator are assumed statistically independent of PMPC states. They are modeled by a Poisson point process with mean  $\mu_{\text{fa}n}$  and PDF  $f_{\text{fa}}(\mathbf{z}_{m,n})$ , which is assumed to factorize as  $f_{\text{fa}}(\mathbf{z}_{m,n}) = f_{\text{fa}d}(z_{dm,n})f_{\text{fa}\varphi}(z_{\varphi m,n})f_{\text{fa}u}(z_{um,n})$ , where  $f_{\text{fa}d}(z_{dm,n}) = 1/d_{\text{max}}$  and  $f_{\text{fa}\varphi}(z_{\varphi m,n}) = 1/2\pi$  are assumed to be uniform on  $[0, d_{\text{max}}]$  and on  $[0, 2\pi)$ , respectively. With noise only, the Rician PDF in (9) degenerates to a Rayleigh PDF, thus the false alarm PDF  $f_{\text{fa}u}(z_{um,n})$  of the normalized amplitude is given as  $f_{\text{fa}u}(z_{um,n}) = 2z_{um,n} \exp(-z_{um,n}^2)/p_{\text{fa}}$  for  $z_{um,n} > \sqrt{u_{\text{de}}}$  where  $p_{\text{fa}} = \exp(-u_{\text{de}})$  denotes the false alarm probability [28, Ch. 1.6.7]. The amplitude information can significantly improve the detectability of MPCs with low component SNRs as shown in Section VII-B2 using very challenging simulation setups (see Fig. 5).

The MNFA  $\mu_{\text{fa}n}$  is assumed unknown, time-varying, and automatically adapted online in the proposed algorithm. It evolves across time according to the state-transition PDF  $f(\mu_{\text{fa}n}|\mu_{\text{fa}n-1})$ . The state vector for all times up to  $n$  is given as  $\boldsymbol{\mu}_{\text{fa}1:n} \triangleq [\mu_{\text{fa}1} \cdots \mu_{\text{fa}n}]^T$ .

#### D. New PMPCs

Newly detected PMPCs at time  $n$ , i.e., PMPCs that generate measurements for the first time at time  $n$ , are modeled by a Poisson point process with mean  $\mu_n$  and PDF  $f_n(\bar{\mathbf{x}}_{m,n})$ . The mean  $\mu_n$  is assumed to be a known constant. Following [8], [29], newly detected PMPCs are represented by new PMPC states  $\bar{\mathbf{y}}_{m,n} \triangleq [\bar{\mathbf{x}}_{m,n}^T \bar{\mathbf{r}}_{m,n}]^T$ ,  $m \in \{1, \dots, M_n\}$ . Each new PMPC  $\bar{\mathbf{y}}_{m,n}$  corresponds to a measurement  $\mathbf{z}_{m,n}$ , thus the number of new PMPCs at time  $n$  equals to the number of measurements  $M_n$ . Here,  $\bar{\mathbf{r}}_{m,n} = 1$  means that the measurement  $\mathbf{z}_{m,n}$  was generated by a newly detected PMPC. The state vector of all new PMPCs at time  $n$  is given by  $\bar{\mathbf{y}}_n \triangleq [\bar{\mathbf{y}}_{1,n}^T \cdots \bar{\mathbf{y}}_{M_n,n}^T]^T$  and state vector for all times up to  $n$  by  $\bar{\mathbf{y}}_{1:n} \triangleq [\bar{\mathbf{y}}_1^T \cdots \bar{\mathbf{y}}_n^T]^T$ . The new PMPCs become legacy PMPCs at time  $n+1$ , accordingly the number of legacy PMPCs is updated as  $K_n = K_{n-1} + M_n$ . (The number of PMPCs is bounded by a pruning operation as it is detailed in Section IV-B.) The vector containing all PMPC states at time  $n$  is given by  $\mathbf{y}_n \triangleq [\mathbf{y}_n^T \bar{\mathbf{y}}_n^T]^T$ , where  $\mathbf{y}_{k,n}$  with  $k \in \{1, \dots, K_n\}$ , and state vector for all times up to  $n$  by  $\mathbf{y}_{1:n} \triangleq [\mathbf{y}_1^T \cdots \mathbf{y}_n^T]^T$ .

#### E. Data Association Uncertainty

Estimation of multiple PMPC states is complicated by the DA uncertainty, i.e., it is unknown which measurement  $\mathbf{z}_{m,n}$  originated from which PMPC. Furthermore, it is not known if a measurement did not originate from a PMPC (false alarm), or if a PMPC did not generate any measurement (missed detection). The associations between measurements and legacy PMPCs are described by the PMPC-oriented association vector  $\mathbf{a}_n \triangleq [a_{1,n} \cdots a_{K_{n-1},n}]^T$  with entries  $a_{k,n} \triangleq m \in \{1, \dots, M_n\}$ , if legacy PMPC  $k$  generates measurement  $m$ , or  $a_{k,n} \triangleq 0$ , if legacy PMPC  $k$  does not generate any measurement. In line with [8], [29], [41], the associations can be equivalently described by a measurement-oriented association vector  $\mathbf{b}_n \triangleq [b_{1,n} \cdots b_{M_n,n}]^T$  with en-

tries  $b_{m,n} \triangleq k \in \{1, \dots, K_{n-1}\}$ , if measurement  $m$  is generated by legacy PMPC  $k$ , or  $b_{m,n} \triangleq 0$ , if measurement  $m$  is not generated by any legacy PMPC. Furthermore, we assume that at any time  $n$ , each PMPC can generate at most one measurement, and each measurement can be generated by at most one PMPC [8], [29], [41]. This is enforced by the exclusion functions  $\Psi(\mathbf{a}_n, \mathbf{b}_n)$  and  $\Gamma_{\mathbf{a}_n}(\bar{\mathbf{r}}_{m,n})$ . The function  $\Psi(\mathbf{a}_n, \mathbf{b}_n) = \prod_{k=1}^{K_{n-1}} \prod_{m=1}^{M_n} \psi(a_{k,n}, b_{m,n})$  is defined as  $\psi(a_{k,n}, b_{m,n}) = 0$ , if  $a_{k,n} = m$  and  $b_{m,n} \neq k$  or  $b_{m,n} = k$  and  $a_{k,n} \neq m$ , otherwise it equals 1. The function  $\Gamma_{\mathbf{a}_n}(\bar{\mathbf{r}}_{m,n}) = 0$ , if  $\bar{\mathbf{r}}_{m,n} = 1$  and  $a_{k,n} = m$ , otherwise it equals 1. The ‘‘redundant formulation’’ of using  $\mathbf{a}_n$  together with  $\mathbf{b}_n$  is the key to make the algorithm scalable for large numbers of PMPCs and measurements. The association vectors for all times up to  $n$  are given by  $\mathbf{a}_{1:n} \triangleq [\mathbf{a}_1^T \cdots \mathbf{a}_n^T]^T$  and  $\mathbf{b}_{1:n} \triangleq [\mathbf{b}_1^T \cdots \mathbf{b}_n^T]^T$ . A figure that conceptually illustrates the DAs between measurements and PMPCs is given in [38].

### IV. JOINT POSTERIOR PDF AND PROBLEM FORMULATION

#### A. Joint Posterior PDF and Factor Graph

Here, we assume that the measurements  $\mathbf{z}_{1:n} \triangleq [z_1^T, \dots, z_n^T]^T$  for all times up to  $n$  are observed and thus fixed. By using common assumptions [8], [28], [29], the joint posterior PDF of  $\mathbf{y}_{1:n}$ ,  $\mathbf{a}_{1:n}$ ,  $\mathbf{b}_{1:n}$ ,  $\boldsymbol{\mu}_{\text{fa}1:n}$ , and  $\mathbf{m}_{1:n}$  conditioned on the observed measurement vector  $\mathbf{z}_{1:n}$  is given by

$$\begin{aligned} & f(\mathbf{y}_{1:n}, \mathbf{a}_{1:n}, \mathbf{b}_{1:n}, \boldsymbol{\mu}_{\text{fa}1:n}, \mathbf{m}_{1:n} | \mathbf{z}_{1:n}) \\ &= f(\underline{\mathbf{y}}_{1:n}, \bar{\mathbf{y}}_{1:n}, \mathbf{a}_{1:n}, \mathbf{b}_{1:n}, \boldsymbol{\mu}_{\text{fa}1:n}, \mathbf{m}_{1:n} | \mathbf{z}_{1:n}) \\ &\propto f(\mathbf{z}_{1:n} | \underline{\mathbf{y}}_{1:n}, \bar{\mathbf{y}}_{1:n}, \mathbf{a}_{1:n}, \mathbf{b}_{1:n}, \mathbf{m}_{1:n}) \\ &\quad \times f(\underline{\mathbf{y}}_{1:n}, \bar{\mathbf{y}}_{1:n}, \mathbf{a}_{1:n}, \mathbf{b}_{1:n}, \boldsymbol{\mu}_{\text{fa}1:n}, \mathbf{m}_{1:n}). \end{aligned} \quad (10)$$

After inserting the expressions (42) and (52) and performing some simple manipulations, the joint posterior PDF in (10) can be rewritten as

$$\begin{aligned} & f(\underline{\mathbf{y}}_{1:n}, \bar{\mathbf{y}}_{1:n}, \mathbf{a}_{1:n}, \mathbf{b}_{1:n}, \boldsymbol{\mu}_{\text{fa}1:n}, \mathbf{m}_{1:n} | \mathbf{z}_{1:n}) \\ &\propto f(\boldsymbol{\mu}_{\text{fa}1}) \prod_{l=1}^{M_1} h(\bar{\mathbf{y}}_{l,1}, b_{l,1}, \mu_{\text{fa}1}; \mathbf{z}_1) \\ &\quad \times \prod_{n'=2}^n f(\mu_{\text{fa}n'} | \mu_{\text{fa}n'-1}) \left( \prod_{k'=1}^{K_{n'-1}} f(\underline{\mathbf{y}}_{k',n'} | \mathbf{y}_{k',n'-1}) \right) \\ &\quad \times \left( \prod_{k=1}^{K_{n'-1}} g(\underline{\mathbf{y}}_{k,n'}, a_{k,n'}, \mu_{\text{fa}n'}; \mathbf{z}_{n'}) \prod_{m=1}^{M_{n'}} \psi(a_{k,n'}, b_{m,n'}) \right) \\ &\quad \times \left( \prod_{m'=1}^{M_{n'}} h(\bar{\mathbf{y}}_{m',n'}, b_{m',n'}, \mu_{\text{fa}n'}; \mathbf{z}_{n'}) \right) \end{aligned} \quad (11)$$

where the functions  $g(\underline{\mathbf{y}}_{k,n}, a_{k,n}, \mu_{\text{fa}n}; \mathbf{z}_n)$  and  $h(\bar{\mathbf{y}}_{m,n}, b_{m,n}, \mu_{\text{fa}n}; \mathbf{z}_n)$  will be discussed next.

The pseudo likelihood functions  $g(\underline{\mathbf{y}}_{k,n}, a_{k,n}, \mu_{\text{fa}n}; \mathbf{z}_n) = g(\underline{\mathbf{x}}_{k,n}, \underline{\mathbf{r}}_{k,n}, a_{k,n}, \mu_{\text{fa}n}; \mathbf{z}_n)$  and  $h(\bar{\mathbf{y}}_{m,n}, b_{m,n}, \mu_{\text{fa}n}; \mathbf{z}_n) = h(\bar{\mathbf{x}}_{m,n}, \bar{\mathbf{r}}_{m,n}, b_{m,n}, \mu_{\text{fa}n}; \mathbf{z}_n)$  are given by

$$g(\underline{\mathbf{x}}_{k,n}, \underline{\mathbf{r}}_{k,n} = 1, a_{k,n}, \mu_{\text{fa}n}; \mathbf{z}_n)$$

$$= \begin{cases} \frac{n(\mu_{\text{fa}_n})f(\mathbf{z}_{m,n}|\underline{\mathbf{x}}_{k,n})p_d(\underline{u}_{k,n})}{\mu_{\text{fa}_n}f_{\text{fa}}(\mathbf{z}_{m,n})}, & a_{k,n} = m \\ n(\mu_{\text{fa}_n})(1 - p_d(\underline{u}_{k,n})), & a_{k,n} = 0 \end{cases} \quad (12)$$

and  $g(\underline{\mathbf{x}}_{k,n}, \underline{r}_{k,n} = 0, a_{k,n}, \mu_{\text{fa}_n}; \mathbf{z}_n) = \bar{1}(a_{k,n})n(\mu_{\text{fa}_n})$  with a factor related to MNFA  $n(\mu_{\text{fa}_n}) \triangleq (e^{-\mu_{\text{fa}_n} \mu_{\text{fa}_n}^{M_n}})^{1/(K_{n-1}+M_n)}$  and by

$$h(\bar{\mathbf{x}}_{m,n}, \bar{r}_{m,n} = 1, b_{m,n}, \mu_{\text{fa}_n}; \mathbf{z}_n) = \begin{cases} 0, & b_{m,n} = k \\ \frac{n(\mu_{\text{fa}_n})\mu_n f_n(\bar{\mathbf{x}}_{m,n})f(\mathbf{z}_{m,n}|\bar{\mathbf{x}}_{m,n})}{\mu_{\text{fa}_n}f_{\text{fa}}(\mathbf{z}_{m,n})}, & b_{m,n} = 0 \end{cases} \quad (13)$$

and  $h(\bar{\mathbf{x}}_{m,n}, \bar{r}_{m,n} = 0, b_{m,n}, \mu_{\text{fa}_n}; \mathbf{z}_n) = n(\mu_{\text{fa}_n})$ , respectively. The factor graph [42], [43] representing the factorization in (11) is shown in Fig. 1. The detailed derivations of the joint posterior PDF in (11) and the pseudo likelihood functions in (12) and (13) are provided in the Appendix in Section A, Section B, and Section C.

### B. PMPC Detection and State Estimation

The problem considered is the sequential detection of PMPCs and estimation of their states  $\mathbf{y}_{k,n}$ ,  $k \in \{1, \dots, K_{n-1} + M_n\}$  along with the estimation of the MNFA  $\mu_{\text{fa}_n}$  based on the measurement vector  $\mathbf{z}_{1:n}$ . This relies on the marginal posterior existence probabilities  $p(r_{k,n} = 1|\mathbf{z}_{1:n})$ , the marginal posterior PDFs  $f(\mathbf{x}_{k,n}|r_{k,n} = 1, \mathbf{z}_{1:n})$  and  $f(\mu_{\text{fa}_n}|\mathbf{z}_{1:n})$ . More specifically, a PMPC is detected if  $p(r_{k,n} = 1|\mathbf{z}_{1:n}) > p_{\text{de}}$  [44], where  $p_{\text{de}}$  is the existence probability threshold not to be confused with  $u_{\text{de}}$  the detection threshold of the snapshot-based estimator. The probabilities  $p(r_{k,n} = 1|\mathbf{z}_{1:n})$  are obtained from the marginal posterior PDFs of the PMPC states,  $f(\mathbf{y}_{k,n}|\mathbf{z}_{1:n}) = f(\mathbf{x}_{k,n}, r_{k,n}|\mathbf{z}_{1:n})$ , according to

$$p(r_{k,n} = 1|\mathbf{z}_{1:n}) = \langle f(\mathbf{x}_{k,n}, r_{k,n} = 1|\mathbf{z}_{1:n}) \rangle_{1_{\mathbb{R}^5 \times 1}(\mathbf{x}_{k,n})} \quad (14)$$

and the marginal posterior PDFs  $f(\mathbf{x}_{k,n}|r_{k,n} = 1, \mathbf{z}_{1:n})$  are obtained from  $f(\mathbf{x}_{k,n}, r_{k,n}|\mathbf{z}_{1:n})$  as

$$f(\mathbf{x}_{k,n}|r_{k,n} = 1, \mathbf{z}_{1:n}) = \frac{f(\mathbf{x}_{k,n}, r_{k,n} = 1|\mathbf{z}_{1:n})}{p(r_{k,n} = 1|\mathbf{z}_{1:n})}. \quad (15)$$

The number of detected PMPCs represents the estimated NoM given by  $\hat{L}_n$ . The states  $\mathbf{u}_{k,n}$  and  $\boldsymbol{\theta}_{k,n}$  of the detected PMPCs are estimated by means of the minimum mean-square error (MMSE) estimator [45], i.e.,

$$\mathbf{u}_{k,n}^{\text{MMSE}} \triangleq \langle \mathbf{u}_{k,n} \rangle_{f(\mathbf{x}_{k,n}|r_{k,n}=1, \mathbf{z}_{1:n})} \quad (16)$$

$$\boldsymbol{\theta}_{k,n}^{\text{MMSE}} \triangleq \langle \boldsymbol{\theta}_{k,n} \rangle_{f(\mathbf{x}_{k,n}|r_{k,n}=1, \mathbf{z}_{1:n})} \quad (17)$$

with  $\boldsymbol{\theta}_{k,n}^{\text{MMSE}} = [d_{k,n}^{\text{MMSE}} \varphi_{k,n}^{\text{MMSE}}]^T \in \mathbb{R}^{2 \times 1}$ , respectively. Note that the estimated component SNRs is given by  $\text{SNR}_{k,n}^{\text{MMSE}} = (u_{k,n}^{\text{MMSE}})^2$ . Finally, the estimate of the MNFA  $\mu_{\text{fa}_n}$  is given by

$$\mu_{\text{fa}_n}^{\text{MMSE}} \triangleq \langle \mu_{\text{fa}_n} \rangle_{f(\mu_{\text{fa}_n}|\mathbf{z}_{1:n})}. \quad (18)$$

To initialize the dispersion parameters of the snapshot-based channel estimator (see Section II-B), the prior PDF is assumed to be Gaussian with vector-valued mean given by the MMSE estimate  $\boldsymbol{\theta}_{k,n-1}^{\text{MMSE}} \in \mathbb{R}^{2 \times 1}$  and covariance matrix  $\boldsymbol{\Sigma}_{k,n-1} = \text{diag}\{\sigma_{d_{k,n-1}}^{\text{MMSE}}, \sigma_{\varphi_{k,n-1}}^{\text{MMSE}}\} \in \mathbb{R}^{2 \times 2}$  of the parameters with  $k \in \{1, \dots, \hat{L}_{n-1}\}$ , where  $\sigma_{d_{k,n}}^{\text{MMSE}} = (\langle (d_{k,n} - d_{k,n}^{\text{MMSE}})^2 \rangle_{f(\mathbf{x}_{k,n}|r_{k,n}=1, \mathbf{z}_{1:n})})^{\frac{1}{2}}$  and  $\sigma_{\varphi_{k,n}}^{\text{MMSE}} = (\langle (\varphi_{k,n} - \varphi_{k,n}^{\text{MMSE}})^2 \rangle_{f(\mathbf{x}_{k,n}|r_{k,n}=1, \mathbf{z}_{1:n})})^{\frac{1}{2}}$ .

As the number of PMPCs grows with time  $n$  (at each time by  $K_n = K_{n-1} + M_n$ ), PMPCs with  $p(r_{k,n} = 1|\mathbf{z}_{1:n})$  below a threshold  $p_{\text{pr}}$  are removed from the state space (“pruned”).

### V. THE PROPOSED SUM-PRODUCT ALGORITHM

The posterior PDFs  $f(\mathbf{x}_{k,n}, r_{k,n}|\mathbf{z}_{1:n})$ ,  $f(\bar{\mathbf{x}}_{m,n}, \bar{r}_{m,n}|\mathbf{z}_{1:n})$ , and  $f(\mu_{\text{fa}_n}|\mathbf{z}_{1:n})$  involved in (14), (15) and (18) are marginal PDFs of the joint posterior PDF  $f(\mathbf{y}_{1:n}, \mathbf{a}_{1:n}, \mathbf{b}_{1:n}, \mu_{\text{fa}_{1:n}}, \mathbf{m}_{1:n}|\mathbf{z}_{1:n})$ . Since direct marginalization of the joint posterior PDF is infeasible, we use loopy (iterative) BP [42] by means of the sum-product algorithm rules [42], [43] on the factor graph shown in Fig. 1. Due to the loops inside the factor graph, the resulting beliefs  $\underline{q}(\underline{\mathbf{y}}_{k,n}) = \underline{q}(\underline{\mathbf{x}}_{k,n}, \underline{r}_{k,n})$ ,  $\bar{q}(\bar{\mathbf{y}}_{m,n}) = \bar{q}(\bar{\mathbf{x}}_{m,n}, \bar{r}_{m,n})$ , and  $q(\mu_{\text{fa}_n})$  are only approximations of the respective posterior marginal PDFs, and there is no canonical order in which the messages should be computed [42]. For the proposed algorithm, we specify the following order: (i) messages are not sent backward in time; (ii) iterative message passing is only performed for probabilistic DA at each time  $n$ . Combining the specified order with the generic BP rules for calculating messages and beliefs yields the following calculations at each time  $n$  (which are in parts in line with [8], [29, Ch. III]):

- 1) *Prediction*: First, a prediction step is performed. The prediction for the MNFA is given by

$$\chi(\mu_{\text{fa}_n}) = \langle f(\mu_{\text{fa}_n}|\mu_{\text{fa}_{n-1}}) \rangle_{q(\mu_{\text{fa}_{n-1}})} \quad (19)$$

and for all the legacy PMPCs is given by

$$\begin{aligned} \chi(\underline{\mathbf{x}}_{k,n}, \underline{r}_{k,n}) &= \sum_{\substack{r_{k,n-1} \\ \in \{0,1\}}} \langle f(\underline{\mathbf{x}}_{k,n}, \underline{r}_{k,n}|\underline{\mathbf{x}}_{k,n-1}, r_{k,n-1}) \rangle_{q(\underline{\mathbf{x}}_{k,n-1}, r_{k,n-1})} \end{aligned} \quad (20)$$

where  $q(\mu_{\text{fa}_{n-1}})$  and  $q(\underline{\mathbf{x}}_{k,n-1}, r_{k,n-1})$  were calculated at the previous time  $n-1$ . After substituting the PMPC state-transition PDFs in (20) with (4) and (5), respectively, we obtain the prediction messages for legacy PMPCs as

$$\chi(\underline{\mathbf{x}}_{k,n}, 1) = p_s \langle f(\underline{\mathbf{x}}_{k,n}|\underline{\mathbf{x}}_{k,n-1}) \rangle_{q(\underline{\mathbf{x}}_{k,n-1}, 1)} \quad (21)$$

and  $\chi(\underline{\mathbf{x}}_{k,n}, 0) = \chi_{k,n} f_D(\underline{\mathbf{x}}_{k,n})$  with

$$\chi_{k,n} = (1 - p_s) \langle q(\underline{\mathbf{x}}_{k,n-1}, 1) \rangle_{1_{\mathbb{R}^5 \times 1}(\underline{\mathbf{x}}_{k,n-1})} + \underline{q}_{k,n-1} \quad (22)$$

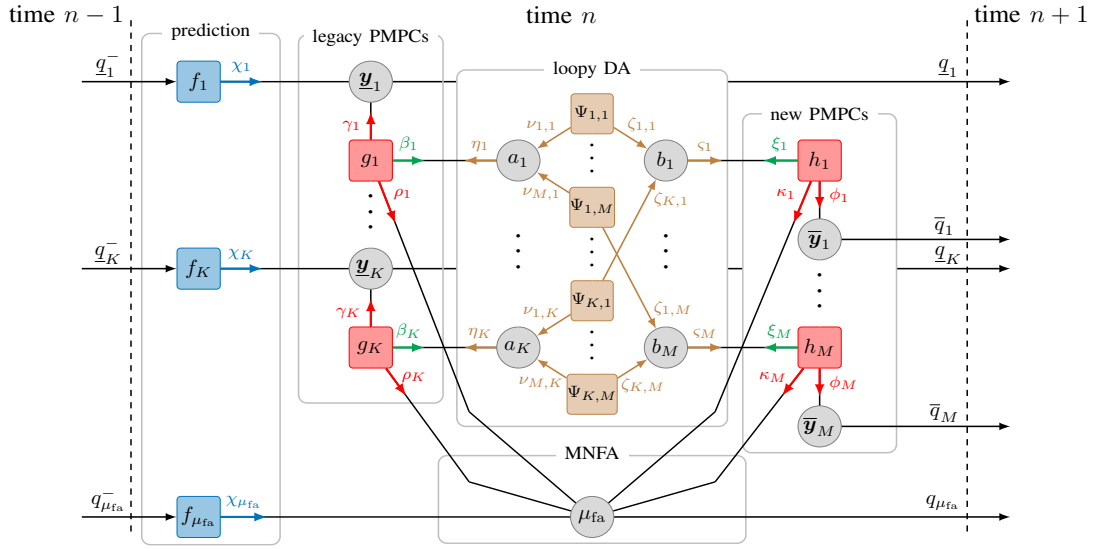


Fig. 1: Factor graph representation of the factorized joint posterior PDF (11). For simplicity, the following short notations are used:  $K \triangleq K_{n-1}$ ,  $M \triangleq M_n$ ; variable nodes:  $a_k \triangleq a_{k,n}$ ,  $b_m \triangleq b_{m,n}$ ,  $\mu_{fa} \triangleq \mu_{fa,n}$ ,  $\underline{\mathbf{y}}_k \triangleq \underline{\mathbf{y}}_{k,n}$ ,  $\bar{\mathbf{y}}_m \triangleq \bar{\mathbf{y}}_{m,n}$ ; factor nodes:  $f_k \triangleq f(\underline{\mathbf{y}}_{k,n} | \underline{\mathbf{y}}_{k,n-1})$ ,  $g_k \triangleq g(\underline{\mathbf{x}}_{k,n}, \underline{\mathbf{r}}_{k,n}, a_{k,n}, \mu_{fa,n}; \mathbf{z}_n)$ ,  $h_m \triangleq h(\bar{\mathbf{x}}_{m,n}, \bar{\mathbf{r}}_{m,n}, b_{m,n}, \mu_{fa,n}; \mathbf{z}_n)$ ,  $f_{\mu_{fa}} \triangleq f(\mu_{fa,n} | \mu_{fa,n-1})$ ,  $\Psi_{k,m} \triangleq \Psi(a_{k,n}, b_{m,n})$ ; prediction:  $\chi_k \triangleq \chi(\underline{\mathbf{x}}_{k,n}, \underline{\mathbf{r}}_{k,n})$ ,  $\chi_{\mu_{fa}} \triangleq \chi(\mu_{fa,n})$ ; measurement evaluation:  $\beta_k \triangleq \beta(a_k)$ ,  $\xi_m \triangleq \xi(b_m)$ ; loopy DA:  $\nu_{m,k} \triangleq \nu_{m \rightarrow k}(a_{k,n})$ ,  $\zeta_{k,m} \triangleq \zeta_{k \rightarrow m}(b_{m,n})$ ,  $\eta_k \triangleq \eta(a_k)$ ,  $\varsigma_m \triangleq \varsigma(b_m)$ ; measurement update:  $\gamma_k \triangleq \gamma(\underline{\mathbf{x}}_{k,n}, \underline{\mathbf{r}}_{k,n})$ ,  $\rho_k \triangleq \rho_k(\mu_{fa,n})$ ,  $\phi_m \triangleq \phi(\bar{\mathbf{x}}_{m,n}, \bar{\mathbf{r}}_{m,n})$ ,  $\kappa_m \triangleq \kappa_m(\mu_{fa,n})$ ; belief calculation:  $\underline{q}_k^- \triangleq \underline{q}(\underline{\mathbf{x}}_{k,n-1}, \underline{\mathbf{r}}_{k,n-1})$ ,  $\underline{q}_k \triangleq \underline{q}(\underline{\mathbf{x}}_{k,n}, \underline{\mathbf{r}}_{k,n})$ ,  $\bar{q}_m \triangleq \bar{q}(\bar{\mathbf{x}}_{m,n}, \bar{\mathbf{r}}_{m,n})$ ,  $\bar{q}_m^- \triangleq \bar{q}(\mu_{fa,n-1})$ ,  $q_{\mu_{fa}} \triangleq q(\mu_{fa,n})$ .

where  $\chi_{k,n} \triangleq \langle \chi(\underline{\mathbf{x}}_{k,n}, 0) \rangle_{1_{\mathbb{R}^5 \times 1}(\underline{\mathbf{x}}_{k,n})}$  and  $\underline{q}_{k,n-1} \triangleq \langle \underline{q}(\underline{\mathbf{x}}_{k,n-1}, 0) \rangle_{1_{\mathbb{R}^5 \times 1}(\underline{\mathbf{x}}_{k,n-1})}$ . After the prediction step, the following steps are performed for all legacy and new PMPCs in parallel:

- 2) *Measurement Evaluation*: For legacy PMPCs, the messages  $\beta(a_{k,n})$  passed from the factor nodes  $g(\underline{\mathbf{x}}_{k,n}, \underline{\mathbf{r}}_{k,n}, a_{k,n}, \mu_{fa,n}; \mathbf{z}_n)$  to the PMPC-oriented DA variable nodes  $a_{k,n}$  are calculated by

$$\begin{aligned} \beta(a_{k,n}) = & \langle \langle g(\underline{\mathbf{x}}_{k,n}, 1, a_{k,n}, \mu_{fa,n}; \mathbf{z}_n) \rangle_{\chi(\underline{\mathbf{x}}_{k,n}, 1)} \rangle_{\chi(\mu_{fa,n})} \\ & + \bar{1}(a_{k,n}) \langle \langle \chi(\underline{\mathbf{x}}_{k,n}, 0) \rangle_{\chi(\mu_{fa,n})} \rangle_{1_{\mathbb{R}^5 \times 1}(\underline{\mathbf{x}}_{k,n})}. \end{aligned} \quad (23)$$

For new PMPCs, the messages  $\xi(b_{m,n})$  passed from the factor nodes  $h(\bar{\mathbf{x}}_{m,n}, \bar{\mathbf{r}}_{m,n}, b_{m,n}, \mu_{fa,n}; \mathbf{z}_n)$  to the measurement-oriented DA variable nodes  $b_{m,n}$  are calculated according to

$$\xi(b_{m,n}) = \sum_{\bar{\mathbf{r}}_{m,n} \in \{0,1\}} \langle \langle h(\bar{\mathbf{x}}_{m,n}, \bar{\mathbf{r}}_{m,n}, b_{m,n}, \mu_{fa,n}; \mathbf{z}_n) \rangle_{1_{\mathbb{R}^5 \times 1}(\bar{\mathbf{x}}_{m,n})} \rangle_{\chi(\mu_{fa,n})}. \quad (24)$$

More specifically, for  $b_{m,n} = k$  it becomes  $\xi(b_{m,n}) = \langle n(\mu_{fa,n}) \chi(\mu_{fa,n}) \rangle_{1_{\mathbb{R}}(\mu_{fa,n})}$  and for  $b_{m,n} = 0$  it becomes

$$\begin{aligned} \xi(b_{m,n}) = & \langle n(\mu_{fa,n}) \chi(\mu_{fa,n}) \rangle_{1_{\mathbb{R}}(\mu_{fa,n})} \\ & + \langle \langle \frac{\mu_n f_n(\bar{\mathbf{x}}_{m,n}) n(\mu_{fa,n})}{\mu_{fa,n}} \rangle_{\chi(\mu_{fa,n})} \rangle_{1_{\mathbb{R}^5 \times 1}(\bar{\mathbf{x}}_{m,n})} \\ & \times \langle \langle \frac{f(\mathbf{z}_{m,n} | \bar{\mathbf{x}}_{m,n})}{f_{fa}(\mathbf{z}_{m,n})} \rangle_{\chi(\mu_{fa,n})} \rangle_{1_{\mathbb{R}^5 \times 1}(\bar{\mathbf{x}}_{m,n})}. \end{aligned} \quad (25)$$

- 3) *Iterative Probabilistic DA*: With the messages  $\beta(a_{k,n})$  and  $\xi(b_{m,n})$ , the probabilistic DA messages  $\eta(a_{k,n})$  and  $\varsigma(b_{m,n})$  are obtained with an efficient loopy BP-based algorithm as shown in [8], [35], [41]

$$\eta(a_{k,n}) = \prod_{m=1}^{M_n} \nu_{\psi_{m \rightarrow k}}^{(p)}(a_{k,n}) \quad (26)$$

$$\varsigma(b_{m,n}) = \prod_{k=1}^{K_{n-1}} \zeta_{\psi_{k \rightarrow m}}^{(p)}(b_{m,n}) \quad (27)$$

where  $\nu_{\psi_{m \rightarrow k}}^{(p)}(a_{k,n})$  and  $\zeta_{\psi_{k \rightarrow m}}^{(p)}(b_{m,n})$  denote the messages passed from  $\psi(a_{k,n}, b_{m,n})$  to the variable nodes  $a_{k,n}$  and  $b_{m,n}$  at each iteration  $p \in \{1, \dots, P\}$ , respectively.

- 4) *Measurement Update*: For legacy PMPCs, the messages  $\gamma(\underline{\mathbf{x}}_{k,n}, \underline{\mathbf{r}}_{k,n})$  passed from the factor nodes  $g(\underline{\mathbf{x}}_{k,n}, \underline{\mathbf{r}}_{k,n}, a_{k,n}, \mu_{fa,n}; \mathbf{z}_n)$  to the variable nodes  $\underline{\mathbf{y}}_{k,n}$  are calculated by

$$\gamma(\underline{\mathbf{x}}_{k,n}, 1) = \sum_{a_{k,n}=0}^{M_n} \eta(a_{k,n}) \langle g(\underline{\mathbf{x}}_{k,n}, 1, a_{k,n}, \mu_{fa,n}; \mathbf{z}_n) \rangle_{\chi(\mu_{fa,n})} \quad (28)$$

and  $\gamma(\underline{\mathbf{x}}_{k,n}, 0) = \gamma_{k,n} f_D(\underline{\mathbf{x}}_{k,n})$  with

$$\begin{aligned} \gamma_{k,n} &= \langle \gamma(\underline{\mathbf{x}}_{k,n}, 0) \rangle_{1_{\mathbb{R}^5 \times 1}(\underline{\mathbf{x}}_{k,n})} \\ &= \eta(0) \langle n(\mu_{fa,n}) \rangle_{\chi(\mu_{fa,n})}. \end{aligned} \quad (29)$$

For new PMPCs, the messages  $\phi(\bar{\mathbf{x}}_{m,n}, \bar{\mathbf{r}}_{m,n})$  passed

from the factor nodes  $h(\bar{\mathbf{x}}_{m,n}, \bar{\mathbf{r}}_{m,n}, b_{m,n}, \mu_{\text{fa}_n}; \mathbf{z}_n)$  to the variable nodes  $\bar{\mathbf{y}}_{m,n}$  are calculated by

$$\phi(\bar{\mathbf{x}}_{m,n}, 1) = \varsigma(0) \langle h(\bar{\mathbf{x}}_{m,n}, 1, b_{m,n}, \mu_{\text{fa}_n}; \mathbf{z}_n) \rangle_{\chi(\mu_{\text{fa}_n})} \quad (30)$$

and  $\phi(\bar{\mathbf{x}}_{m,n}, 0) = \phi_{m,n} f_{\text{D}}(\bar{\mathbf{x}}_{m,n})$  with

$$\begin{aligned} \phi_{m,n} &\triangleq \langle \phi(\bar{\mathbf{x}}_{m,n}, 0) \rangle_{1_{\mathbb{R}^5 \times 1}(\bar{\mathbf{x}}_{m,n})} \\ &= \sum_{b_{m,n}=0}^{K_{n-1}} \varsigma(b_{m,n}) \langle n(\mu_{\text{fa}_n}) \rangle_{\chi(\mu_{\text{fa}_n})}. \end{aligned} \quad (31)$$

For the MNFA  $\mu_{\text{fa}_n}$ , the messages  $\rho_k(\mu_{\text{fa}_n})$  and  $\kappa_m(\mu_{\text{fa}_n})$  passed from the factor nodes  $g(\mathbf{x}_{k,n}, \mathbf{r}_{k,n}, a_{k,n}, \mu_{\text{fa}_n}; \mathbf{z}_n)$  and  $h(\bar{\mathbf{x}}_{m,n}, \bar{\mathbf{r}}_{m,n}, b_{m,n}, \mu_{\text{fa}_n}; \mathbf{z}_n)$ , respectively, to the variable node  $\mu_{\text{fa}_n}$  are calculated by

$$\rho_k(\mu_{\text{fa}_n}) = \sum_{a_{k,n}=0}^{M_n} \eta(a_{k,n}) \sum_{\mathbf{r}_{k,n} \in \{0,1\}} \langle g(\mathbf{x}_{k,n}, \mathbf{r}_{k,n}, a_{k,n}, \mu_{\text{fa}_n}; \mathbf{z}_n) \rangle_{\chi(\mathbf{x}_{k,n}, \mathbf{r}_{k,n})} \quad (32)$$

and

$$\begin{aligned} \kappa_m(\mu_{\text{fa}_n}) &= n(\mu_{\text{fa}_n}) \varsigma(0) \left\langle \frac{\mu_n f(\mathbf{z}_{m,n} | \bar{\mathbf{x}}_{m,n})}{\mu_{\text{fa}_n} f_{\text{fa}}(\mathbf{z}_{m,n})} \right\rangle_{f_n(\bar{\mathbf{x}}_{m,n})} \\ &\quad + \sum_{b_{m,n}=0}^{K_{n-1}} \varsigma(b_{m,n}) n(\mu_{\text{fa}_n}). \end{aligned} \quad (33)$$

- 5) *Belief Calculation*: With all the messages above, the approximations of the marginal posterior PDFs needed for the MMSE estimations in Section IV-B are calculated as follows. The beliefs  $q(\mathbf{y}_{k,n}) = q(\mathbf{x}_{k,n}, \mathbf{r}_{k,n})$  approximating the marginal posterior PDFs  $f(\mathbf{y}_{k,n} | \mathbf{z}_{1:n}) = f(\mathbf{x}_{k,n}, \mathbf{r}_{k,n} | \mathbf{z}_{1:n})$  for legacy PMPCs are obtained as

$$q(\mathbf{x}_{k,n}, 1) = \frac{1}{C_{k,n}} \chi(\mathbf{x}_{k,n}, 1) \gamma(\mathbf{x}_{k,n}, 1) \quad (34)$$

and  $q(\mathbf{x}_{k,n}, 0) = \underline{q}_{k,n} f_{\text{D}}(\mathbf{x}_{k,n})$  with  $\underline{q}_{k,n} = \frac{1}{C_{k,n}} \chi_{k,n} \gamma_{k,n}$ . The normalization constant is given as  $C_{k,n} = \langle \gamma(\mathbf{x}_{k,n}, 1) \rangle_{\chi(\mathbf{x}_{k,n}, 1)} + \chi_{k,n} \gamma_{k,n}$ . The beliefs  $\bar{q}(\bar{\mathbf{y}}_{m,n}) = \bar{q}(\bar{\mathbf{x}}_{m,n}, \bar{\mathbf{r}}_{m,n})$  approximating the marginal posterior PDFs  $f(\bar{\mathbf{y}}_{m,n} | \mathbf{z}_{1:n}) = f(\bar{\mathbf{x}}_{m,n}, \bar{\mathbf{r}}_{m,n} | \mathbf{z}_{1:n})$  for new PMPCs are obtained as

$$\bar{q}(\bar{\mathbf{x}}_{m,n}, 1) = \frac{1}{C_{m,n}} \phi(\bar{\mathbf{x}}_{m,n}, 1) \quad (35)$$

and  $\bar{q}(\bar{\mathbf{x}}_{m,n}, 0) = \bar{q}_{m,n} f_{\text{D}}(\bar{\mathbf{x}}_{m,n})$  with  $\bar{q}_{m,n} = \frac{1}{C_{m,n}} \phi_{m,n}$ . The normalization constant is given as  $C_{m,n} = \langle \phi(\bar{\mathbf{x}}_{m,n}, 1) \rangle_{1_{\mathbb{R}^5 \times 1}(\bar{\mathbf{x}}_{m,n})} + \phi_{m,n}$ . Finally, the belief  $q(\mu_{\text{fa}_n})$  approximating the marginal posterior PDF

$f(\mu_{\text{fa}_n} | \mathbf{z}_{1:n})$  for the MNFA is obtained as

$$q(\mu_{\text{fa}_n}) = \chi(\mu_{\text{fa}_n}) \prod_{k=1}^{K_{n-1}} \rho_k(\mu_{\text{fa}_n}) \prod_{m=1}^{M_n} \kappa_m(\mu_{\text{fa}_n}). \quad (36)$$

## VI. PARTICLE-BASED IMPLEMENTATION

Since integrations involved in the calculations of the messages and beliefs cannot be obtained analytically, we use a computationally efficient sequential particle-based message passing implementation which provides approximate computations. In what follows, we present particle-based implementations for MNFA related steps (19), (32), (33) and (36). The implementation of all other steps in Section V, and the calculation of posterior existence probabilities of PMPCs are performed in line with [35, Section VI]. Similarly to [8], our implementation uses a ‘‘stacked state’’ [46] comprising the PMPC states and the MNFA state.

- 1) *Prediction*: The belief  $q(\mu_{\text{fa}_{n-1}})$  calculated at the previous time  $n-1$  is represented by  $J$  particles and weights, i.e.,  $\{\hat{\mu}_{\text{fa}_{n-1}}^{(j)}, \hat{w}_{\text{fa}_{n-1}}^{(j)}\}_{j=1}^J$ . At time  $n$ , for each particle  $\hat{\mu}_{\text{fa}_{n-1}}^{(j)}$ ,  $j \in \{1, \dots, J\}$  one particle  $\mu_{\text{fa}_n}^{(j)}$  with corresponding weight  $w_{\text{fa}_n}^{(j)} = \hat{w}_{\text{fa}_{n-1}}^{(j)}$  is drawn from  $f(\mu_{\text{fa}_n} | \mu_{\text{fa}_{n-1}})$ , and  $\{\mu_{\text{fa}_n}^{(j)}, w_{\text{fa}_n}^{(j)}\}_{j=1}^J$  represent the prediction message  $\chi(\mu_{\text{fa}_n})$  in (19). Note that the proposal distribution underlying the weight calculation is  $f(\mu_{\text{fa}_n} | \mu_{\text{fa}_{n-1}})$ .
- 2) *Measurement Update*: The non-normalized weights corresponding to the messages for legacy PMPCs  $\rho_k(\mu_{\text{fa}_n})$  in (32) and new PMPCs  $\kappa_m(\mu_{\text{fa}_n})$  in (33) are calculated by

$$\begin{aligned} \underline{w}_{\text{fa}_{k,n}}^{(j)} &= \sum_{a_{k,n}=0}^{M_n} \eta(a_{k,n}) g(\mathbf{x}_{k,n}^{(j)}, 1, a_{k,n}, \mu_{\text{fa}_n}^{(j)}; \mathbf{z}_n) \\ &\quad \times w_{k,n}^{(j)} + n(\mu_{\text{fa}_n}^{(j)}) \frac{(1 - \sum_{j=0}^J w_{k,n}^{(j)})}{J} \end{aligned} \quad (37)$$

and

$$\begin{aligned} \bar{w}_{\text{fa}_{m,n}}^{(j)} &= n(\mu_{\text{fa}_n}^{(j)}) \frac{\mu_n f(\mathbf{z}_{m,n} | \bar{\mathbf{x}}_{m,n}^{(j)})}{\mu_{\text{fa}_n}^{(j)} f_{\text{fa}}(\mathbf{z}_{m,n})} f_n(\bar{\mathbf{x}}_{m,n}^{(j)}) \\ &\quad + \sum_{b_{m,n}=0}^{K_{n-1}} \varsigma(b_{m,n}) n(\mu_{\text{fa}_n}^{(j)}) \end{aligned} \quad (38)$$

respectively. The weighted particles  $\{\mathbf{x}_{k,n}^{(j)}, \underline{w}_{k,n}^{(j)}\}_{j=1}^J$  represent the prediction messages  $\chi(\mathbf{x}_{k,n}, \mathbf{r}_{k,n})$  of legacy PMPCs in (20), thus their predicted existence probabilities can be approximated as  $\sum_{j=0}^J \underline{w}_{k,n}^{(j)}$ , and  $(1 - \sum_{j=0}^J \underline{w}_{k,n}^{(j)})/J$  is the weight of particles representing  $\chi(\mathbf{x}_{k,n}, 0)$ . Moreover, the weighted particles  $\{\bar{\mathbf{x}}_{m,n}^{(j)}, \bar{w}_{k,n}^{(j)} = 1/J\}_{j=1}^J$  with equal weights represent the states of new PMPCs.

- 3) *Belief Calculation and State Estimation*: The above approximate messages are further used for calculating

the non-normalized weights corresponding to the belief  $q(\mu_{\text{fa},n})$  in (36), given by

$$w_{\text{fa},n}^{(j)} = w_{\text{fa},n}^{\prime(j)} \prod_{k=1}^{K_{n-1}} \underline{w}_{\text{fa},k,n}^{(j)} \prod_{m=1}^{M_n} \bar{w}_{\text{fa},m,n}^{(j)}. \quad (39)$$

After normalization  $w_{\text{fa},n}^{(j)} = w_{\text{fa},n}^{\prime(j)} / \sum_{j=0}^J w_{\text{fa},n}^{\prime(j)}$ , an approximation of the MMSE state estimate  $\mu_{\text{fa},n}^{\text{MMSE}}$  in (18) is given by

$$\mu_{\text{fa},n}^{\text{MMSE}} \approx \sum_{j=0}^J w_{\text{fa},n}^{(j)} \mu_{\text{fa},n}^{\prime(j)}. \quad (40)$$

To avoid the particle degeneracy effect, a resampling step [35] is performed as a final preparation for the next time  $n+1$  leading to  $\{\hat{\mu}_{\text{fa},n}^{(j)}, \hat{w}_{\text{fa},n}^{(j)} = 1/J\}_{j=1}^J$  representing the belief  $q(\mu_{\text{fa},n})$ . Assuming a fixed number  $P$  of message passing iterations for DA, the computational complexity of calculating the (approximate) marginal posterior PDFs scales only linearly in the number of particles. Moreover, the complexity of the iterative DA given by the operations in (26) and (27) scales as  $O(K_{n-1}M_n)$ , i.e., quadratically in the number of PMPCs [29], [35], [41].

## VII. EXPERIMENTAL RESULTS

The performance of the proposed algorithm is validated using both synthetic and real radio measurements. For synthetic measurements, the performance is further compared with the PCRLB [47] and that of the KEST algorithm [27].

### A. Analysis Setup

1) *Common Simulation Setup*: For synthetic and real measurements, the following setups and parameters are commonly used. We assume that MPC dispersion parameters with according velocities and normalized amplitudes evolve independently across time and to each other. More specifically, the state-transition PDF of  $\underline{\theta}_{k,n}$  (with according velocities  $\underline{v}_{d,k,n}$  and  $\underline{v}_{\varphi,k,n}$ ) is chosen to be a nearly-constant velocity model. The state-transition PDF of the normalized amplitude  $\underline{u}_{k,n}$  is chosen to be  $\underline{u}_{k,n} = u_{k,n-1} + \epsilon_{u,k,n}$ , where the noise  $\epsilon_{u,k,n}$  is independent and identically distributed (iid) across  $k$  and  $n$ , zero-mean, and Gaussian with variance  $\sigma_{u,k,n}^2$ . Based on the models above, the state-transition PDF of legacy PMPC state  $\underline{x}_{k,n}$  is collectively given as  $\underline{x}_{k,n} = \mathbf{F}\underline{x}_{k,n-1} + \mathbf{\Gamma}\epsilon_n$ , where the transition matrices  $\mathbf{F} \in \mathbb{R}^{5 \times 5}$  and  $\mathbf{\Gamma} \in \mathbb{R}^{5 \times 3}$  are formulated as in [23], [48, Section 6.3.2] with sampling period  $\Delta T = 1$  s. The driving process  $\epsilon_n \in \mathbb{R}^{3 \times 1}$  is iid across  $k$  and  $n$ , zero-mean and Gaussian with covariance matrix  $\text{diag}\{\sigma_d^2, \sigma_\varphi^2, \sigma_{u,k,n}^2\}$ . In addition, the state-transition PDF of the MNFA  $\mu_{\text{fa},n}$  is given as  $\mu_{\text{fa},n} = \mu_{\text{fa},n-1} + \epsilon_{\text{fa},n}$ , where  $\epsilon_{\text{fa},n}$  is iid across  $n$ , zero-mean, and Gaussian with variance  $\sigma_{\text{fa}}^2$ .<sup>4</sup> For computational efficiency of the particle-based implementation,

<sup>4</sup>Incorporating the interacting multiple model (IMM) [37] into the algorithm can help to resolve the motion uncertainties of the unknown variable states, therefore the demand on presetting and tuning of noise variances for the state-transition PDFs can be relaxed. However, it is out of the scope of this paper and can be considered as a future extension.

the likelihood function (9) of the normalized amplitude is approximated by a truncated Gaussian PDF, i.e.,

$$f(z_{u,m,n}|u_{k,n}) = \frac{1}{\sigma_{u,k,n}\sqrt{2\pi}} \exp\left(\frac{-(z_{u,m,n}-u_{k,n})^2}{2\sigma_{u,k,n}^2}\right) p_d(u_{k,n}) \quad (41)$$

for  $z_{u,m,n} > \sqrt{u_{\text{de}}}$ , where  $p_d(u_{k,n}) = Q((\sqrt{u_{\text{de}}} - u_{k,n})/\sigma_{u,k,n})$  is the CDF of Gaussian distribution. The birth PDF of a new PMPCs  $f_n(\bar{\mathbf{x}}_{m,n}) = 1/(2\pi d_{\text{max}})$  is assumed to be uniform on  $[0, 2\pi d_{\text{max}})$ . The particles for the initial state  $\bar{\mathbf{x}}_{m,n}$  of a new PMPC are drawn from a 5-D Gaussian PDF with means  $[z_{d,m,n} z_{\varphi,m,n} z_{u,m,n} 0 0]^T$  and variances  $[\sigma_{d,m,n}^2 \sigma_{\varphi,m,n}^2 \sigma_{u,m,n}^2 \sigma_{v_d}^2 \sigma_{v_\varphi}^2]^T$ , where  $\sigma_{d,m,n}^2$ ,  $\sigma_{\varphi,m,n}^2$  and  $\sigma_{u,m,n}^2$  are calculated using the amplitude measurements  $z_{u,m,n}$  (see Section III-C). The particles for the initial MNFA  $\mu_{\text{fa},n}$  state are drawn from a Gaussian PDF with mean  $M_1/2$  and variance  $\sigma_{\text{fa},\text{ini}}^2$ . The other simulation parameters are as follows: the survival probability  $p_s = 0.999$ , the existence probability threshold  $p_{\text{de}} = 0.5$ , the pruning threshold  $p_{\text{pr}} = 10^{-4}$ , the mean number of newly detected MPCs  $\mu_n = 0.008$ , the maximum number of message passing iterations for DA  $P = 5000$  and the PDFs of the states are represented by  $J = 10000$  particles each.

For each simulation run, AWGN is generated with noise variance  $\sigma^2$  specified by the SNR output defined as  $\text{SNR}_{1\text{m}} = 10 \log_{10} \left( \frac{|\alpha_{\text{LoS}}|^2 \|\mathbf{s}_{\text{LoS}}\|^2}{\sigma^2} \right)$ , where the amplitude  $\alpha_{\text{LoS}}$  and the signal vector  $\mathbf{s}_{\text{LoS}}$  of the line-of-sight (LoS) path are computed at 1 m distance. For comparability with other papers presenting parametric channel estimation methods as for example [21], [25], [27], we also define the input SNR, i.e.,  $\text{SNR}_{1\text{m}}^{\text{in}} = \text{SNR}_{1\text{m}} - 10 \log_{10}(N_s H)$ , the input component SNRs  $\text{SNR}_{l,n}^{\text{in}} = 10 \log_{10}(\widehat{\text{SNR}}_{l,n}/(N_s H))$  and the input detection threshold  $u_{\text{de}}^{\text{in}} = 10 \log_{10}(u_{\text{de}}/(N_s H))$  excluding the array and frequency sample gain.

2) *Metrics*: The performance of different methods is measured using the optimal subpattern assignment (OSPA) metric [49], which can efficiently capture the estimation errors of the NoM and MPC states when comparing with the true MPC states at each time. We use OSPA metric order 2 and cutoff parameters 0.1 m and  $10^\circ$  for distance and AoA respectively, where cutoff parameters denote the weightings of how the metric penalizes the NoM estimation errors as opposed to MPC state estimation errors. In addition, we compute the PCRLB [47] as a performance benchmark. The error bounds for distance and AoA at time  $n$  are given as  $\varepsilon_{d,n} = (\text{tr}[\mathbf{J}_{p,n}^{-1}]_{1:L_n})^{\frac{1}{2}}$  and  $\varepsilon_{\varphi,n} = (\text{tr}[\mathbf{J}_{p,n}^{-1}]_{L_n+1:2L_n})^{\frac{1}{2}}$ , where  $\mathbf{J}_{p,n}$  denotes the posterior Fisher information matrix (FIM). The mean OSPA (MOSPA) errors, mean error bounds (MEBs), and the mean estimate of each unknown variable are obtained by averaging over all simulation runs.

### B. Performance for Synthetic Measurements

We assume that the static single-antenna Tx transmits  $\bar{s}(t)$  to the Rx equipped with a  $3 \times 3$  uniform rectangular array with inter-element spacing of 2 cm. Over 364 time steps, 7 MPCs with different lifetimes and time-varying distances and AoAs

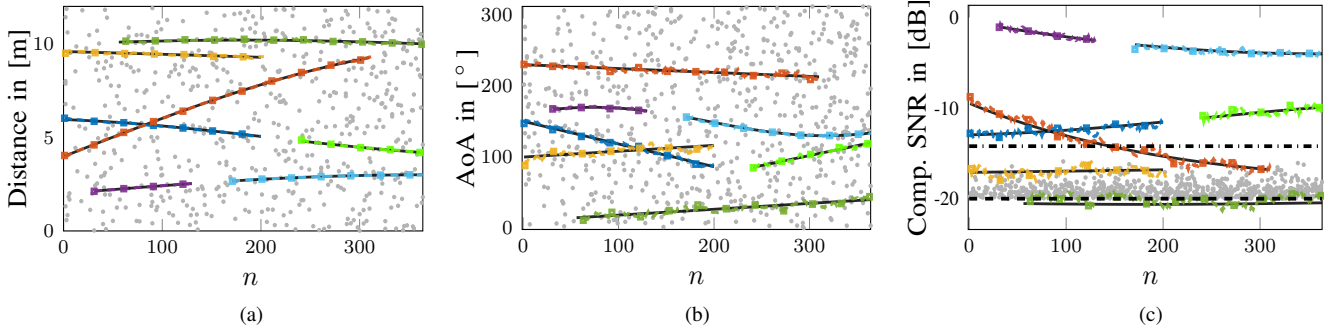


Fig. 2: Results for fully synthetic measurements with the proposed algorithm given  $\text{SNR}_{1m}^{\text{in}} = 5.4$  dB. The estimates of (a) distances, (b) AoAs, and (c) input component SNRs. The black solid lines denote the true MPC parameters. The gray dots denote the false alarm measurements. The estimates of different MPCs are denoted with densely-dashed lines with square markers in different colors. The horizontal dashed and dash-dotted lines in (c) indicate the detection thresholds of  $-20$  dB and  $-14.4$  dB, respectively.

were synthesized. The amplitude of each MPC is assumed to follow free-space pathloss and is attenuated by 3 dB after each reflection. Furthermore, we have designed two intersections between MPCs in their distance and AoA parameters at time  $n = 83$  and  $n = 125$ , respectively. For the intersection at time  $n = 83$ , the distances intersect simultaneously with the amplitudes. For the transmit signal  $\tilde{s}(t)$ , we use a root-raised-cosine pulse with a roll-off factor of 0.6 and pulse duration of  $T_p = 2$  ns (bandwidth of 500 MHz) at center frequency of  $f_c = 6$  GHz. With sampling period  $T_s = 1.25$  ns, the number of samples per array element is  $N_s = 46$ . In [11], [39], a detection threshold  $u_{\text{de}}^{\text{in}}$  is determined for SR-SBL channel estimation algorithms for single-snapshot wideband MIMO measurements. Given the signal parameters, number of antennas, and array-layout as defined above, this detection threshold  $u_{\text{de}}^{\text{in}}$  for a chosen false alarm probability of  $10^{-2}$  is given as  $-14.4$  dB. MPCs below  $u_{\text{de}}^{\text{in}}$  are mostly miss detected and therefore barely utilized as measurements in the proposed algorithm. To support the detection and estimation of low SNR MPCs, the detection threshold can be relaxed. This will inevitably bring more false alarm measurements, but the proposed algorithm can efficiently filter them out even under low  $\text{SNR}_{1m}^{\text{in}}$  conditions as shown in the following experimental results. We performed 100 simulation runs for each  $\text{SNR}_{1m}^{\text{in}} \in \{-0.6, 2.4, 3.9, 5.4, 8.4, 13.4, 15.4, 18.4\}$  dB with parameters:  $d_{\text{max}} = 17$  m,  $\sigma_{\text{fa,ini}} = 0.5$ ,  $\sigma_{\text{fa}} = 0.15$ ,  $\sigma_d = 0.002$  m/s<sup>2</sup>,  $\sigma_\varphi = 0.17^\circ$ /s<sup>2</sup>,  $\sigma_{u_{k,n}} = 0.02 u_{k,n-1}^{\text{MMSE}}$ ,  $\sigma_{v_d} = 0.01$  m/s,  $\sigma_{v_\varphi} = 0.6^\circ$ /s.<sup>5</sup> Note that the first four  $\text{SNR}_{1m}^{\text{in}}$  values represent extreme testing setups, where the true component SNRs (output) of some MPCs are even below or close to 0 dB SNR output.

1) *Fully Synthetic Measurements*: First, we present the simulation results using fully synthetic measurements without involving the snapshot-based channel estimator. In each simulation run, MPC-oriented measurements were generated by adding Gaussian noises to the true MPC parameters,

<sup>5</sup>The heuristic approach to scale the standard deviation  $\sigma_{u_{k,n}}$  by the MMSE estimates  $u_{k,n-1}^{\text{MMSE}}$  was chosen since the range of normalized amplitude values tends to be very large.

where the noise variances were state-dependent and computed as in Section III-C. In addition, false alarm measurements were generated with increasing MNFA  $\mu_{\text{fa},n}$  from 1.5 to 3. More specifically, the distances and AoAs of false alarm measurements were drawn from uniform distributions in the validation region, and the norm amplitudes were generated with Rayleigh distribution with squared scale parameter 1/2 using a detection threshold of  $u_{\text{de}}^{\text{in}} = -20$  dB.

Fig. 2 shows the results of an exemplary simulation run given  $\text{SNR}_{1m}^{\text{in}} = 5.4$  dB. It is seen that the proposed algorithm exhibits high detection and estimation accuracy for medium and high SNR MPCs. The “weakest” MPC—with component SNR below the detection threshold of  $-20$  dB—is stably detected shortly after the beginning although the related measurements are mostly miss detected in the SR-SBL. In addition, the proposed algorithm excellently copes with intersecting MPCs. Fig. 3 further presents the MOSPA errors and the mean estimates of the NoM and the MNFA given  $\text{SNR}_{1m}^{\text{in}} = \{5.4, 13.4, 18.4\}$  dB. Given medium and high  $\text{SNR}_{1m}^{\text{in}}$  values, the NoM is accurately estimated and the MOSPA errors attain the MEBs. For distance, AoA and component SNR, the MOSPA errors are mostly below 2 cm,  $2^\circ$  and  $-35$  dB, respectively. Given  $\text{SNR}_{1m}^{\text{in}} = 5.4$  dB, the MOSPA errors remain on the MEB-levels mostly, despite a few peaks due to the underestimated NoM. Furthermore, the slow varying MNFA is accurately estimated for all conditions. Additional simulation results for fully synthetic measurements with fast varying MNFA are provided in Appendix E1.

2) *Synthetic Radio Measurements*: Next, we show the overall performance of the proposed two-stage algorithm by involving the snapshot-based channel estimator. In each simulation run, radio measurements were synthesized by applying true MPC parameters to the radio signal model (2) with given  $\text{SNR}_{1m}^{\text{in}}$ . The measurements  $z_{m,n}$  at each time  $n$  were provided by a snapshot-based SR-SBL channel estimator in line with the implementation in [30]. We relaxed the detection threshold to  $u_{\text{de}}^{\text{in}} = -18$  dB for  $\text{SNR}_{1m}^{\text{in}}$  values above 5 dB and  $u_{\text{de}}^{\text{in}} = -20$  dB otherwise. For comparison, we implemented the KEST algorithm according to [19] and [27] which per-

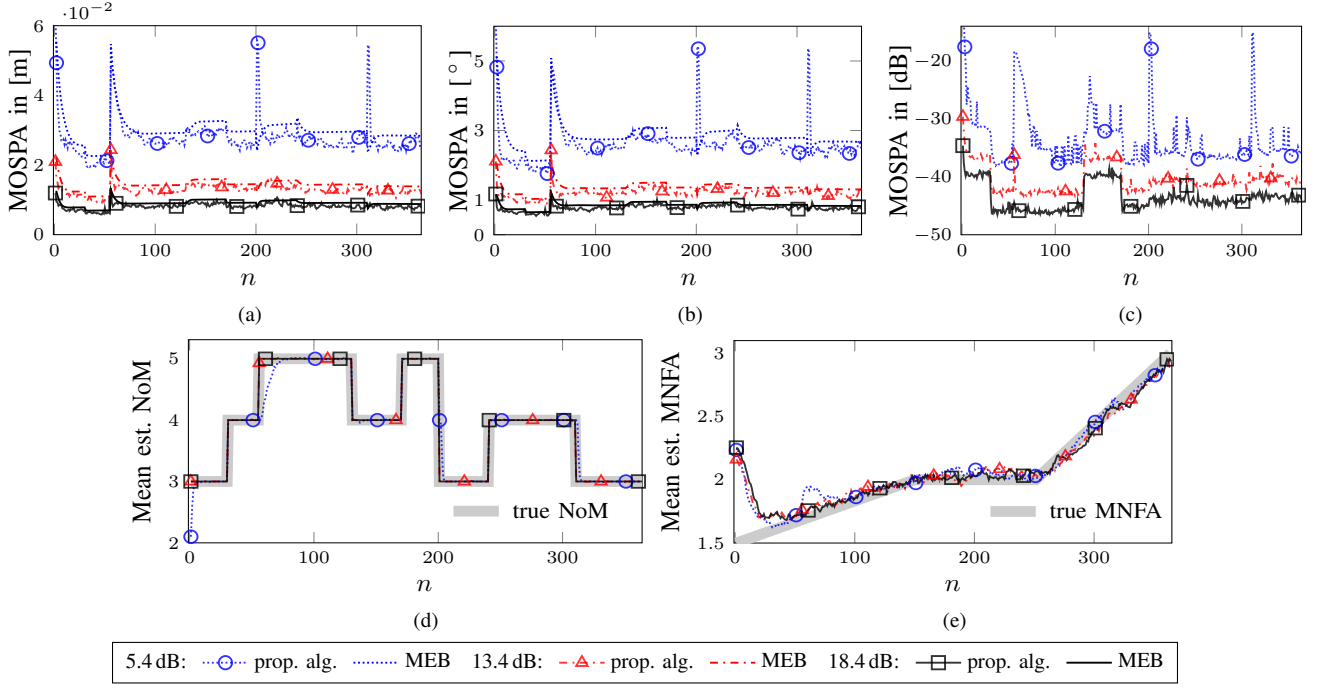


Fig. 3: Results for fully synthetic measurements with the proposed algorithm (prop. alg.) given  $\text{SNR}_{1m}^{\text{in}} = \{5.4, 13.4, 18.4\}$  dB. MOSPA errors of the estimated (a) distances, (b) AoAs, and (c) input component SNRs. Mean estimates of the NoM (d) and the MNFA (e).

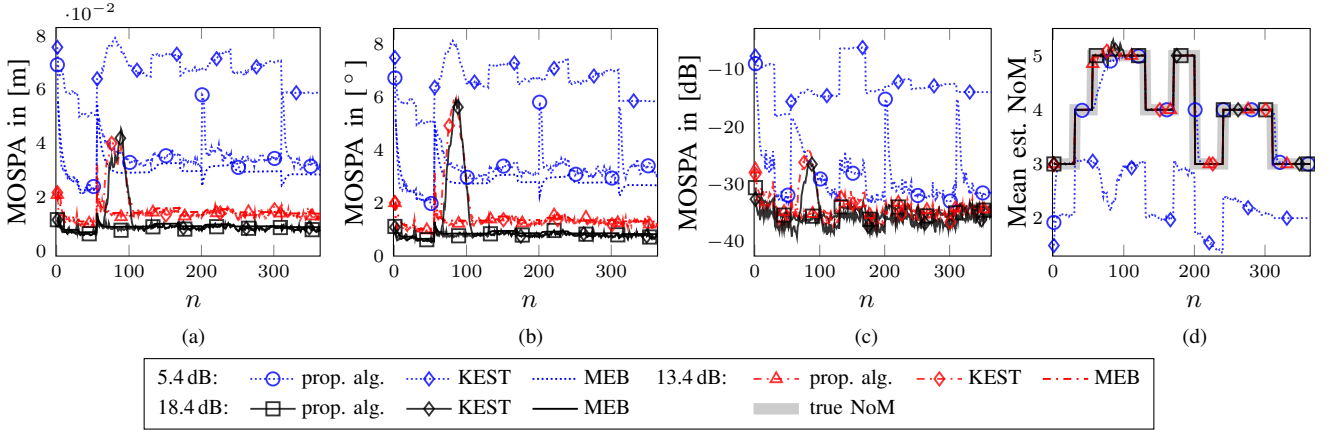


Fig. 4: Results for synthetic radio measurements given  $\text{SNR}_{1m}^{\text{in}} = \{5.4, 13.4, 18.4\}$  dB. MOSPA errors of the estimated (a) distances, (b) AoAs, and (c) input component SNRs. Mean estimates of the NoM (d).

forms detection of MPCs and sequential estimation of their distances, AoAs and amplitudes. For NoM estimation in the KEST algorithm, the penalty factor for a NoM change was set to  $p_{\text{chg}} = 0.1$ , and the penalty  $p_{\text{ord}}$  for a higher NoM was chosen according to the MDL principle [19], [27].

For comparison between the proposed algorithm and the KEST algorithm of an exemplary simulation run, the reader is referred to Appendix E2. Fig. 4 shows the MOSPA errors, MEBs and the mean estimate of the NoM for each  $\text{SNR}_{1m}^{\text{in}} \in \{5.4, 13.4, 18.4\}$  dB. The peaks of MOSPA errors indicate the NoM estimation errors which mostly happen when there is MPC birth or death. For medium and high  $\text{SNR}_{1m}^{\text{in}}$ , it shows that the MOSPA errors of the proposed algorithm are mostly below 2 cm,  $2^\circ$  and  $-35$  dB respectively for distance,

AoA and input component SNR. The KEST algorithm shows comparable results except for the high error peaks around the intersecting MPCs at time  $n = 83$ . At low SNR, the MOSPA errors versus time  $n$  of the proposed algorithm are slightly above the MEBs since the “weakest” MPCs—with component SNRs well below the relaxed detection thresholds—are occasionally not detected, however, the KEST algorithm has much larger MOSPA errors, since it almost never detects these MPCs.

Finally, Fig. 5 shows component SNRs of the MPCs, the mean cardinality error [49] in the NoM, and MOSPA errors averaged over all time steps versus SNR ( $\text{SNR}_{1m}^{\text{in}} \in \{-0.6, 2.4, 3.9, 5.4, 8.4, 13.4, 15.4, 18.4\}$  dB). Fig. 5a shows that quite a few of the MPCs have component SNRs that

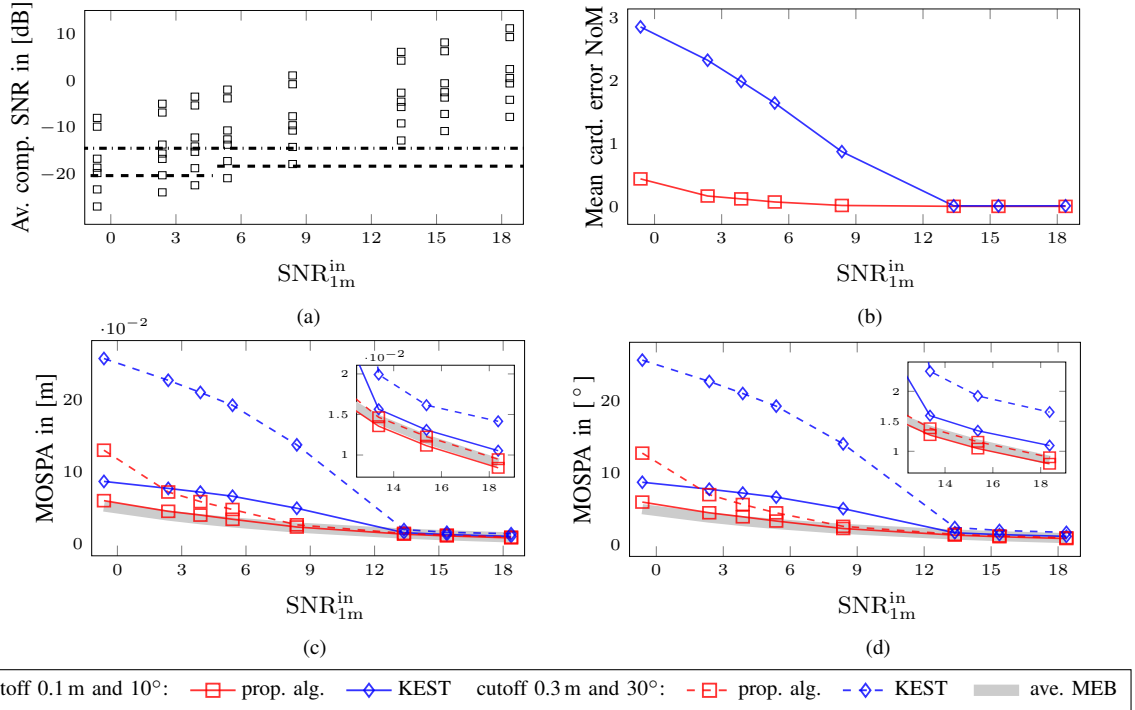


Fig. 5: Results for synthetic radio measurements: The average (averaged over all time steps) (a) true input component SNRs of 7 MPCs, (b) mean cardinality error of the NoM, and (c) and (d) MOSPA errors and MEBs. In (a), the dash-dotted line indicates the theoretical detection threshold of  $-14.4$  dB, and the dashed lines indicate the relaxed detection thresholds of  $-20$  dB and  $-18$  dB, respectively.

are below the relaxed detection thresholds (some even far below the theoretical threshold) for the first five  $\text{SNR}_{1m}^{\text{in}}$  values. These MPCs are mostly miss detected by the KEST algorithm, leading to a much higher mean cardinality error [49] as shown in Fig. 5b and therefore also to much higher MOSPA errors, as shown in Fig. 5c and Fig. 5d, than that of the proposed algorithm. By setting the cutoff parameters to larger values, i.e., 0.3 m and  $30^\circ$ , the mean cardinality error and MOSPA errors are better visualized. At high  $\text{SNR}_{1m}^{\text{in}}$  values both algorithms mostly detected all MPCs. However, the proposed algorithm still outperforms the KEST algorithm since its MOSPA errors are lower when MPCs are intersecting. In summary, the proposed algorithm outperforms the KEST algorithm in all testing conditions and attains the MEBs for  $\text{SNR}_{1m}^{\text{in}}$  above 5 dB. A study of the runtimes for both algorithms can be found in Appendix E3. For instance, the runtimes per time step (for MATLAB implementations) of both algorithms for  $\text{SNR}_{1m}^{\text{in}} = 18.4$  dB, obtained by averaging over all simulation runs and time steps, are both approximately 2 s/step.

### C. Performance for Real UWB Radio Measurements

For further validation of the proposed algorithm, we use real radio measurements collected in a seminar room at TU Graz, Austria. The floor plan is depicted in Fig. 6, including the positions of the static Tx and a few mirror images of the Tx, i.e., virtual anchors (VAs), which model the MPCs due to specular reflections. More details about the measurement environment and VA calculations can be found in [8], [50], [51].

On the Tx side, a dipole-like antenna with an approximately uniform radiation pattern in the azimuth plane and zeros in the floor and ceiling directions was used. At each Rx position, a same antenna was mounted on a plotter and moved yielding a virtual uniform rectangular array with an inter-element spacing of 2 cm. The UWB signals are measured at 100 Rx positions along a 2 m trajectory using an M-sequence correlative channel sounder with frequency range 3.1–10.6 GHz. We selected a subband with bandwidth  $B = 1/T_p$  using filtering with a root-raised-cosine pulse with a roll-off factor of 0.6 and pulse duration  $T_p$  at center frequency of  $f_c = 6$  GHz. The following two measurement setups are used: (i) *setup-1*:  $T_p = 2$  ns,  $B = 0.5$  GHz,  $N_s = 94$ ,  $3 \times 3$  array,  $\text{SNR}_{1m}^{\text{in}} = 0.7$  dB,  $u_{\text{de}}^{\text{in}} = -16$  dB; (ii) *setup-2*:  $T_p = 1$  ns,  $B = 1$  GHz,  $N_s = 187$ ,  $5 \times 5$  array,  $\text{SNR}_{1m}^{\text{in}} = -6.7$  dB,  $u_{\text{de}}^{\text{in}} = -20$  dB. Since no significant AWGN was observed from the filtered signal, artificial AWGN generated with  $\text{SNR}_{1m}$  was added. The simulation parameters are as follows:  $d_{\text{max}} = 30$  m,  $\sigma_d = 0.03$  m/s<sup>2</sup>,  $\sigma_\varphi = 1^\circ$ /s<sup>2</sup>,  $\underline{\sigma}_{u_{k,n}} = 0.1 u_{k,n-1}^{\text{MMSE}}$ ,  $\sigma_{\text{fa}} = 1$ ,  $\sigma_{\text{vd}} = 0.1$  m/s,  $\sigma_{\text{v}\varphi} = 6^\circ$ /s.

Fig. 7 shows the estimated delays and AoAs of the detected MPCs for *setup-1* and *setup-2*. The backgrounds of Fig. 7a and Fig. 7b are the delay and angular power spectra versus time respectively for *setup-2*, where the peaks and variations representing individual MPC paths are readily visible in delay domain with good resolution capability of UWB signals, but hardly resolved in angular domain with limited array aperture. As can be observed, some distinct peaks align with the MPC

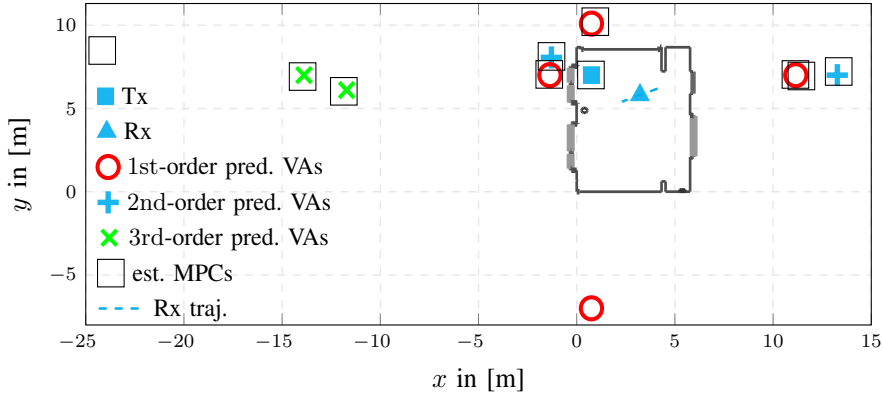


Fig. 6: Floor plan of the measurement environment and the results of the proposed algorithm using real radio measurements of *setup-2* (1 GHz bandwidth,  $5 \times 5$  array) at time  $n = 50$ . For each of the 10 detected MPCs, the estimated state is transformed into a two-dim. coordinate and associated with a geometrically calculated VA.

paths predicted with up to 3rd-order geometrically expected VAs, and related to the estimated MPC paths highlighted with markers in Fig. 7c and Fig. 7d for *setup-1* and in Fig. 7e and Fig. 7f for *setup-2*. The intersecting 1st-order MPCs and a few short-lived MPCs around 5 m are nearby in both delay and angular domains. They are better resolved for *setup-2* with larger signal bandwidth and array size, however oscillation on the estimates still exist especially in the angular domain as for *setup-1*. Fig. 6 zooms into the performance of a single snapshot for *setup-2*, where the MMSE estimates of the detected MPC states at time  $n = 50$  after being transformed into two-dimensional coordinates are shown. Within the 10 detected MPCs, the LoS component and MPCs related to the three 1st-order VAs w.r.t. surrounding walls are accurately estimated. Most of the other detected MPCs are also well explained by some higher order VAs (up to order five). However, due to imperfect antenna-calibration leading to time-dispersive system response, “ghost” components are sometimes detected alongside significant MPCs. The estimated MPCs associated with the 2nd and the upper 3rd-order VAs are related to the complex room structure in the left-upper corner. Note that the lower wall has high attenuation coefficient and therefore no related MPCs are detected (as for example the MPC related to the 1st-order VA of the lower wall which has parameters around 14 m and  $270^\circ$ ). The estimated MNFAs for both measurement setups converge rapidly and remain around one over time. The small and stable values can be explained by the high detection threshold  $u_{\text{de}}^{\text{in}}$  used in the SBL channel estimator and the static measurement scenario. The proposed algorithm is capable of detecting MPCs and estimating their parameters that very well resemble the geometry, and capturing their dynamic behaviors related to the surrounding environment.

### VIII. CONCLUSIONS

We proposed a BP-based algorithm for sequential detection and estimation of MPC parameters based on radio signals, which adopts a two-stage structure combining a snapshot-based SR-SBL channel estimator with a BP-based sequential detection and estimation algorithm. Using amplitude information and the augmentation of PMPC states with a binary exist-

tence variable enable the reliable detection of “weak” MPCs with very low component SNRs. Simulation results using synthetic measurements show that the algorithm excellently copes with a high number of false alarm measurements and intersecting MPCs with parameters nearby in the dispersion space. It is capable of estimating the parameters of MPCs on PCRLB-levels even for low SNR MPCs. We have shown that the performance of the proposed algorithm compares well to existing state-of-the-art algorithms for high SNR MPCs, but it significantly outperforms them for medium and low SNR MPCs. The results using real radio measurements show that the algorithm demonstrates excellent performance in challenging indoor-environments by detecting many geometry-related MPCs up to reflection-order five and estimating their dispersion parameters with high accuracy. Possible directions for future research include extending the proposed algorithm to a more general inhomogeneous false alarm intensity [52] coping with false alarms resulting from model mismatches in the radio signal such as DMC or incorporating correlations between measurements [53].

### IX. ACKNOWLEDGMENT

The authors would like to thank Dr. Florian Meyer and Prof. Bernard H. Fleury for carefully reading the manuscript and insightful comments.

### APPENDIX

We provide derivations of the joint prior PDF and the joint likelihood function in Section A and Section B respectively, which lead to the factorized expressions of the joint posterior PDF (11) and the pseudo likelihood functions (12) and (13) in Section C. In Section D, we derive the squared scale parameter of the truncated Rician PDF in (9).

#### A. Joint Prior PDF

Before presenting derivations, we first define a few sets as follows:  $\mathcal{D}_{\mathbf{a}_n, \mathbf{r}_n} \triangleq \{k \in \{1, \dots, K_{n-1}\} : \mathbf{r}_{k,n} = 1, a_{k,n} \neq 0\}$  denotes the existing legacy PMPCs set, and  $\mathcal{N}_{\bar{\mathbf{r}}_n} \triangleq \{m \in \{1, \dots, M_n\} : \bar{\mathbf{r}}_{m,n} = 1, b_{m,n} = 0\}$  denotes the existing new PMPCs set. Correspondingly, the sets of non-existing

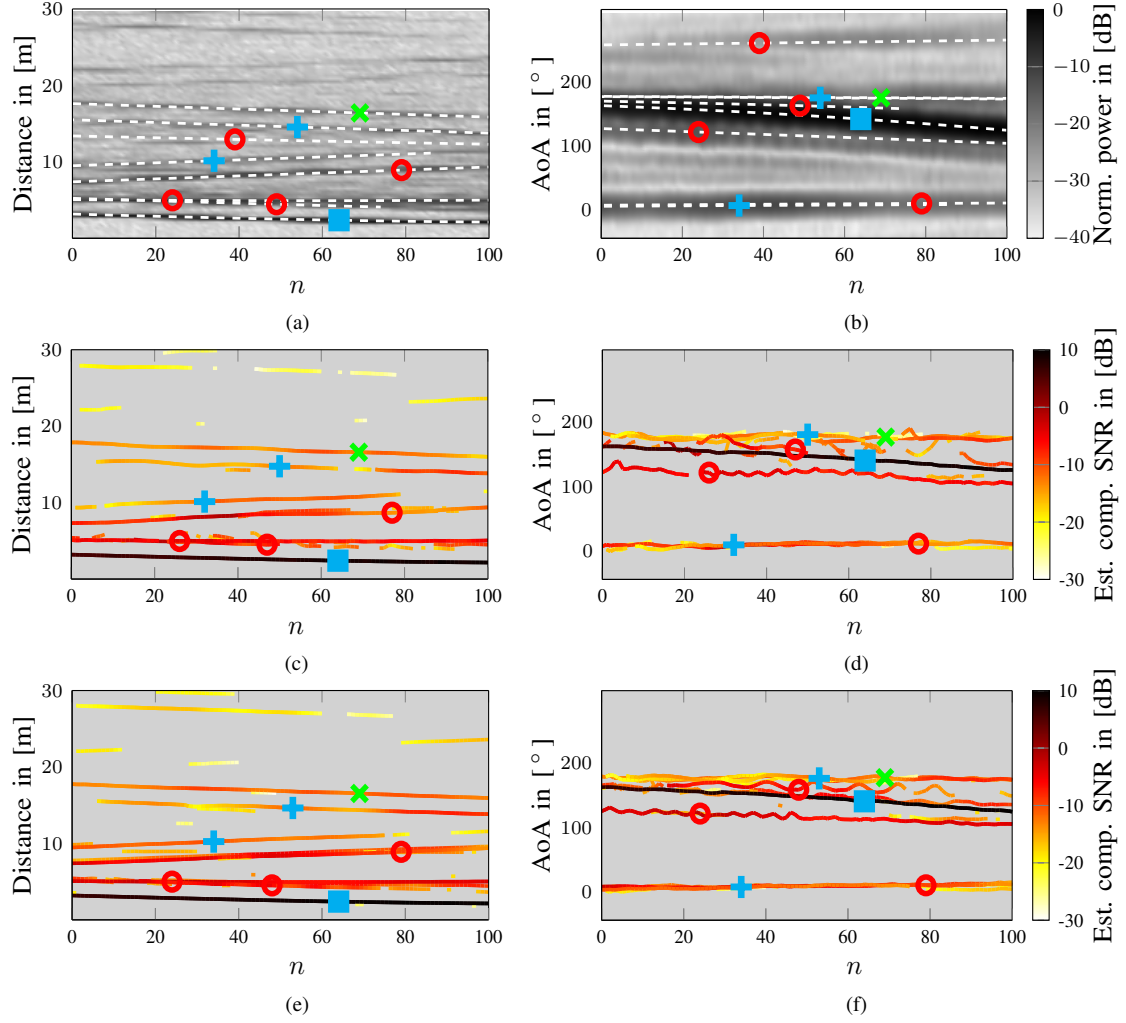


Fig. 7: Results for real radio measurements. (a) and (b) depict the delay and angular power spectra versus time for *setup-2*. Corresponding to the distinct peaks and their variations in the spectra, a few exemplary distance and AoA paths (white dashed lines) are calculated with geometrically expected VAs, of which the orders are highlighted with markers listed in Fig. 6. The distance and AoA estimates of the detected MPCs are shown for *setup-1* in (c) and (d), and for *setup-2* in (e) and (f), among which the estimates associated with the geometrically calculated paths in (a) and (c) are highlighted with markers.

legacy PMPCs are given by  $\bar{\mathcal{D}}_{\mathbf{a}_n, \mathbf{r}_n} \triangleq \{1, \dots, K_{n-1}\} \setminus \mathcal{D}_{\mathbf{a}_n, \mathbf{r}_n}$ , and the sets of non-existing new PMPCs are given as  $\bar{\mathcal{N}}_{\bar{\mathbf{r}}_n} \triangleq \{1, \dots, M_n\} \setminus \mathcal{N}_{\bar{\mathbf{r}}_n}$ . Hence, the number of false alarm measurements can be represented with the sets as  $k_{\text{fa}n} = M_n - |\mathcal{D}_{\mathbf{a}_n, \mathbf{r}_n}| - |\mathcal{N}_{\bar{\mathbf{r}}_n}|$ , and the number of PMPCs states is given as  $K_{n-1} + M_n = |\mathcal{D}_{\mathbf{a}_n, \mathbf{r}_n}| + |\bar{\mathcal{D}}_{\mathbf{a}_n, \mathbf{r}_n}| + |\mathcal{N}_{\bar{\mathbf{r}}_n}| + |\bar{\mathcal{N}}_{\bar{\mathbf{r}}_n}|$ .

Assuming that the new PMPCs states  $\bar{\mathbf{y}}_n$  and the PMPC-oriented association variables  $\mathbf{a}_n$  are conditionally independent given the legacy PMPCs state  $\mathbf{y}_n$ , the joint prior PDF of  $\mathbf{y}_{1:n}$ ,  $\bar{\mathbf{y}}_{1:n}$ ,  $\mathbf{a}_{1:n}$ ,  $\mathbf{b}_{1:n}$ ,  $\boldsymbol{\mu}_{\text{fa}1:n}$ , and the number of the measurements  $\mathbf{m}_{1:n}$  factorizes as

$$\begin{aligned} & f(\mathbf{y}_{1:n}, \mathbf{a}_{1:n}, \mathbf{b}_{1:n}, \boldsymbol{\mu}_{\text{fa}1:n}, \mathbf{m}_{1:n}) \\ &= f(\mathbf{y}_{1:n}, \bar{\mathbf{y}}_{1:n}, \mathbf{a}_{1:n}, \mathbf{b}_{1:n}, \boldsymbol{\mu}_{\text{fa}1:n}, \mathbf{m}_{1:n}) \\ &= f(\boldsymbol{\mu}_{\text{fa}1}) f(\bar{\mathbf{x}}_1 | \bar{\mathbf{r}}_1, M_1) p(\bar{\mathbf{r}}_1, \mathbf{a}_1, \mathbf{b}_1, M_1 | \boldsymbol{\mu}_{\text{fa}1}) \end{aligned}$$

$$\begin{aligned} & \times \prod_{n'=2}^n f(\boldsymbol{\mu}_{\text{fa}n'} | \boldsymbol{\mu}_{\text{fa}n'-1}) \left( \prod_{k=1}^{K_{n'-1}} f(\mathbf{y}_{k,n'} | \mathbf{y}_{k,n'-1}) \right) \\ & \times f(\bar{\mathbf{x}}_n | \bar{\mathbf{r}}_n, M_n) p(\bar{\mathbf{r}}_n, \mathbf{a}_n, \mathbf{b}_n, M_n | \boldsymbol{\mu}_{\text{fa}n}, \mathbf{y}_n) \end{aligned} \quad (42)$$

where  $p(\bar{\mathbf{r}}_1, \mathbf{a}_1, \mathbf{b}_1, M_1 | \boldsymbol{\mu}_{\text{fa}1}, \mathbf{y}_1) = p(\bar{\mathbf{r}}_1, \mathbf{a}_1, \mathbf{b}_1, M_1 | \boldsymbol{\mu}_{\text{fa}1})$  since no legacy PMPCs exist at time  $n = 1$ . We determine the prior PDF of new PMPCs  $f(\bar{\mathbf{x}}_n | \bar{\mathbf{r}}_n, M_n)$  and the joint conditional prior PMF  $p(\bar{\mathbf{r}}_n, \mathbf{a}_n, \mathbf{b}_n, M_n | \boldsymbol{\mu}_{\text{fa}n}, \mathbf{y}_n)$  as follows.

Before the current measurements are observed, the number of measurements  $M_n$  is random. The Poisson PMF of the number of existing new PMPCs evaluated at  $|\mathcal{N}_{\bar{\mathbf{r}}_n}|$  is given by  $p(|\mathcal{N}_{\bar{\mathbf{r}}_n}|) = \mu_n^{|\mathcal{N}_{\bar{\mathbf{r}}_n}|} / |\mathcal{N}_{\bar{\mathbf{r}}_n}|! e^{-\mu_n}$ . The prior PDF of the new PMPC state  $\bar{\mathbf{x}}_n$  conditioned on  $\bar{\mathbf{r}}_n$  and  $M_n$  is expressed as

$$f(\bar{\mathbf{x}}_n | \bar{\mathbf{r}}_n, M_n) = \prod_{m \in \mathcal{N}_{\bar{\mathbf{r}}_n}} f_n(\bar{\mathbf{x}}_{m,n}) \prod_{m' \in \bar{\mathcal{N}}_{\bar{\mathbf{r}}_n}} f_D(\bar{\mathbf{x}}_{m',n}). \quad (43)$$

The PMF for the number of false alarm measurements is given by  $p(k_{\text{fa}n}) = \mu_{\text{fa}n}^{k_{\text{fa}n}} / k_{\text{fa}n}! e^{-\mu_{\text{fa}n}}$ . The joint conditional prior PMF of the binary existence variables of new PMPCs  $\bar{\mathbf{r}}_n \triangleq [\bar{r}_{1,n} \cdots \bar{r}_{M_n,n}]$ , the DA vectors  $\mathbf{a}_n$  and  $\mathbf{b}_n$  and the number of the measurements  $M_n$  conditioned on  $\mu_{\text{fa}n}$  and  $\mathbf{y}_n$  is obtained as [8], [28], [29]

$$\begin{aligned} & p(\bar{\mathbf{r}}_n, \mathbf{a}_n, \mathbf{b}_n, M_n | \mu_{\text{fa}n}, \mathbf{y}_n) \\ &= \chi_{\bar{\mathbf{r}}_n, \mathbf{a}_n, M_n} \left( \prod_{m \in \mathcal{N}_{\bar{\mathbf{r}}_n}} \Gamma_{\mathbf{a}_n}(\bar{r}_{m,n}) \right) \left( \prod_{k \in \mathcal{D}_{\mathbf{a}_n, \mathbf{r}_n}} p_d(\underline{u}_{k,n}) \right) \\ & \times \Psi(\mathbf{a}_n, \mathbf{b}_n) \left( \prod_{k' \in \bar{\mathcal{D}}_{\mathbf{a}_n, \mathbf{r}_n}} (1 - r_{k',n}) p_d(\underline{u}_{k',n}) \right). \end{aligned} \quad (44)$$

The normalization constant  $\chi_{\bar{\mathbf{r}}_n, \mathbf{a}_n, M_n}$  combining the two Poisson PMFs above is given by

$$\begin{aligned} \chi_{\bar{\mathbf{r}}_n, \mathbf{a}_n, M_n} &= (e^{-\mu_n} / M_n!) \left( (\mu_n / \mu_{\text{fa}n})^{|\mathcal{N}_{\bar{\mathbf{r}}_n}|} \mu_{\text{fa}n}^{-|\mathcal{D}_{\mathbf{a}_n, \mathbf{r}_n}|} \right) \\ & \times (e^{-\mu_{\text{fa}n}} \mu_{\text{fa}n}^{M_n}) \end{aligned} \quad (45)$$

where the first part (the terms in the first brackets) is fixed after observing the current measurements given the assumption that the mean number of newly detected PMPCs  $\mu_n$  is a known constant. The second part can be merged with factors in the sets  $\mathcal{N}_{\bar{\mathbf{r}}_n}$  and  $\mathcal{D}_{\mathbf{a}_n, \mathbf{r}_n}$ , respectively. The third part equals to  $n(\mu_{\text{fa}n})^{(K_{n-1} + M_n)}$  where  $n(\mu_{\text{fa}n}) \triangleq (e^{-\mu_{\text{fa}n}} \mu_{\text{fa}n}^{M_n})^{1/(K_{n-1} + M_n)}$  is the MNFA-related normalization constant. The two exclusion functions  $\Psi(\mathbf{a}_n, \mathbf{b}_n)$  and  $\Gamma_{\mathbf{a}_n}(\bar{r}_{m,n}) = 0$  ensure that  $p(\bar{\mathbf{r}}_n, \mathbf{a}_n, \mathbf{b}_n, M_n | \mu_{\text{fa}n}, \mathbf{y}_n) \neq 0$  if and only if a measurement is generated by only one PMPC (either a legacy or a new one), and a PMPC generates no more than one measurement.

The product of the prior PDF of new PMPCs (43) and the joint conditional prior PMF (44) after merging factors can be written up to the normalization constant as

$$\begin{aligned} & p(\bar{\mathbf{r}}_n, \mathbf{a}_n, \mathbf{b}_n, M_n | \mu_{\text{fa}n}, \mathbf{y}_n) f(\bar{\mathbf{x}}_n | \bar{\mathbf{r}}_n, M_n) \\ & \propto \left( \psi(\mathbf{a}_n, \mathbf{b}_n) \prod_{k \in \mathcal{D}_{\mathbf{a}_n, \mathbf{r}_n}} \frac{n(\mu_{\text{fa}n}) p_d(\underline{u}_{k,n})}{\mu_{\text{fa}n}} \right. \\ & \times \left. \prod_{k' \in \bar{\mathcal{D}}_{\mathbf{a}_n, \mathbf{r}_n}} n(\mu_{\text{fa}n}) (\bar{1}(a_{k',n}) - r_{k',n}) p_d(\underline{u}_{k',n}) \right) \\ & \times \left( \prod_{m \in \mathcal{N}_{\bar{\mathbf{r}}_n}} \frac{n(\mu_{\text{fa}n}) \mu_n f_n(\bar{\mathbf{x}}_{m,n})}{\mu_{\text{fa}n}} \Gamma_{\mathbf{a}_n}(\bar{r}_{m,n}) \right. \\ & \times \left. \prod_{m' \in \bar{\mathcal{N}}_{\bar{\mathbf{r}}_n}} n(\mu_{\text{fa}n}) f_D(\bar{\mathbf{x}}_{m',n}) \right). \end{aligned} \quad (46)$$

With some simple manipulations using the definitions of exclusion functions  $\Psi(\mathbf{a}_n, \mathbf{b}_n)$  and  $\Gamma_{\mathbf{a}_n}(\bar{r}_{m,n})$  (see Section III-E), Eq. (46) can be rewritten as the product of factors related to

the legacy PMPCs and to the new PMPCs, respectively, i.e.,

$$\begin{aligned} & p(\bar{\mathbf{r}}_n, \mathbf{a}_n, \mathbf{b}_n, M_n | \mu_{\text{fa}n}, \mathbf{y}_n) f(\bar{\mathbf{x}}_n | \bar{\mathbf{r}}_n, M_n) \\ & \propto \left( \prod_{k=1}^{K_{n-1}} g_1(\underline{\mathbf{y}}_{k,n}, a_{k,n}, \mu_{\text{fa}n}; M_n) \prod_{m=1}^{M_n} \psi(a_{k,n}, b_{m,n}) \right) \\ & \times \left( \prod_{m'=1}^{M_n} h_1(\bar{\mathbf{y}}_{m',n}, b_{m',n}, \mu_{\text{fa}n}; M_n) \right) \end{aligned} \quad (47)$$

with  $g_1(\underline{\mathbf{y}}_{k,n}, a_{k,n}, \mu_{\text{fa}n}; M_n) = g_1(\underline{\mathbf{x}}_{k,n}, r_{k,n}, a_{k,n}, \mu_{\text{fa}n}; M_n)$  given by

$$\begin{aligned} & g_1(\underline{\mathbf{x}}_{k,n}, r_{k,n} = 1, a_{k,n}, \mu_{\text{fa}n}; M_n) \\ & \triangleq \begin{cases} \frac{n(\mu_{\text{fa}n}) p_d(\underline{u}_{k,n})}{\mu_{\text{fa}n}}, & a_{k,n} = m \\ n(\mu_{\text{fa}n}) (1 - p_d(\underline{u}_{k,n})), & a_{k,n} = 0 \end{cases} \end{aligned} \quad (48)$$

and  $g_1(\underline{\mathbf{x}}_{k,n}, r_{k,n} = 0, a_{k,n}, \mu_{\text{fa}n}; M_n) \triangleq \bar{1}(a_{k,n}) n(\mu_{\text{fa}n})$ , and  $h_1(\bar{\mathbf{y}}_{m,n}, b_{m,n}, \mu_{\text{fa}n}; M_n) = h_1(\bar{\mathbf{x}}_{m,n}, \bar{r}_{m,n}, b_{m,n}, \mu_{\text{fa}n}; M_n)$  is given by

$$\begin{aligned} & h_1(\bar{\mathbf{x}}_{m,n}, \bar{r}_{m,n} = 1, b_{m,n}, \mu_{\text{fa}n}; M_n) \\ & \triangleq \begin{cases} 0, & b_{m,n} = k \\ \frac{n(\mu_{\text{fa}n}) \mu_n f_n(\bar{\mathbf{x}}_{m,n})}{\mu_{\text{fa}n}}, & b_{m,n} = 0 \end{cases} \end{aligned} \quad (49)$$

and  $h_1(\bar{\mathbf{x}}_{m,n}, \bar{r}_{m,n} = 0, b_{m,n}, \mu_{\text{fa}n}; M_n) \triangleq n(\mu_{\text{fa}n})$ .

Finally, by inserting (47) into (42), the joint prior PDF can be rewritten as

$$\begin{aligned} & f(\underline{\mathbf{y}}_{1:n}, \bar{\mathbf{y}}_{1:n}, \mathbf{a}_{1:n}, \mathbf{b}_{1:n}, \mu_{\text{fa}1:n}, \mathbf{m}_{1:n}) \\ & \propto f(\mu_{\text{fa}1}) \prod_{l=1}^{M_1} h_1(\bar{\mathbf{y}}_{l,1}, b_{l,1}, \mu_{\text{fa}1}; M_1) \\ & \times \prod_{n'=2}^n f(\mu_{\text{fa}n'} | \mu_{\text{fa}n'-1}) \left( \prod_{k'=1}^{K_{n'-1}} f(\underline{\mathbf{y}}_{k',n'}, b_{k',n'-1}) \right) \\ & \times \left( \prod_{k=1}^{K_{n'-1}} g_1(\underline{\mathbf{y}}_{k,n'}, a_{k,n'}, \mu_{\text{fa}n'}; M_{n'}) \prod_{m=1}^{M_{n'}} \psi(a_{k,n'}, b_{m,n'}) \right) \\ & \times \left( \prod_{m'=1}^{M_{n'}} h_1(\bar{\mathbf{y}}_{m',n'}, b_{m',n'}, \mu_{\text{fa}n'}; M_{n'}) \right). \end{aligned} \quad (50)$$

## B. Joint Likelihood Function

Assume that the measurements  $\mathbf{z}_n$  are independent across  $n$ , the conditional PDF of  $\mathbf{z}_{1:n}$  given  $\underline{\mathbf{y}}_{1:n}, \bar{\mathbf{y}}_{1:n}, \mathbf{a}_{1:n}, \mathbf{b}_{1:n}$ , and the number of measurements  $\mathbf{m}_{1:n}$  is given by

$$\begin{aligned} & f(\mathbf{z}_{1:n} | \underline{\mathbf{y}}_{1:n}, \bar{\mathbf{y}}_{1:n}, \mathbf{a}_{1:n}, \mathbf{b}_{1:n}, \mathbf{m}_{1:n}) \\ & = \prod_{n'=1}^n f(\mathbf{z}_{n'} | \underline{\mathbf{y}}_{n'}, \bar{\mathbf{y}}_{n'}, \mathbf{a}_{n'}, \mathbf{b}_{n'}, M_{n'}). \end{aligned} \quad (51)$$

Note that  $f(\mathbf{z}_1 | \underline{\mathbf{y}}_1, \bar{\mathbf{y}}_1, \mathbf{a}_1, \mathbf{b}_1, M_1) = f(\mathbf{z}_1 | \bar{\mathbf{y}}_1, \mathbf{a}_1, \mathbf{b}_1, M_1)$  since no legacy PMPCs exist at time  $n = 1$ . The conditional PDF  $f(\mathbf{z}_{m,n} | \underline{\mathbf{x}}_{k,n})$  characterizing the statistical relation be-

tween the measurements  $\mathbf{z}_{m,n}$  and the PMPC states  $\mathbf{x}_{k,n}$  is a central element in the conditional PDF of the measurement vector  $\mathbf{z}_n$  given  $\underline{\mathbf{y}}_n, \bar{\mathbf{y}}_n, \mathbf{a}_n, \mathbf{b}_n$ , and the number of the measurements  $M_n$ . Assuming that the measurements  $\mathbf{z}_{m,n}$  are conditionally independent across  $m$  given  $\underline{\mathbf{y}}_{k,n}, \bar{\mathbf{y}}_{m,n}, \mathbf{a}_{k,n}, \mathbf{b}_{m,n}$ , and  $M_n$  [28], Eq. (51) factorizes as

$$\begin{aligned} & f(\mathbf{z}_{1:n} | \underline{\mathbf{y}}_{1:n}, \bar{\mathbf{y}}_{1:n}, \mathbf{a}_{1:n}, \mathbf{b}_{1:n}, \mathbf{m}_{1:n}) \\ &= C(\mathbf{z}_1) \left( \prod_{m \in \mathcal{N}_{\bar{\mathbf{r}}_1}} \frac{f(\mathbf{z}_{m,1} | \bar{\mathbf{x}}_{m,1})}{f_{\text{fa}}(\mathbf{z}_{m,1})} \right) \\ & \times \prod_{n'=2}^n C(\mathbf{z}_{n'}) \left( \prod_{k \in \mathcal{D}_{\mathbf{a}_{n'}, \mathbf{x}_{n'}}} \frac{f(\mathbf{z}_{a_{k,n'}, n'} | \underline{\mathbf{x}}_{k,n'})}{f_{\text{fa}}(\mathbf{z}_{a_{k,n'}, n'})} \right) \\ & \times \left( \prod_{m \in \mathcal{N}_{\bar{\mathbf{r}}_{n'}}} \frac{f(\mathbf{z}_{m,n'} | \bar{\mathbf{x}}_{m,n'})}{f_{\text{fa}}(\mathbf{z}_{m,n'})} \right), \end{aligned} \quad (52)$$

and the conditional PDF at each time  $n \geq 2$  factorizes as [28]

$$\begin{aligned} & f(\mathbf{z}_n | \underline{\mathbf{y}}_n, \bar{\mathbf{y}}_n, \mathbf{a}_n, \mathbf{b}_n, M_n) \\ &= C(\mathbf{z}_n) \left( \prod_{k \in \mathcal{D}_{\mathbf{a}_n, \mathbf{x}_n}} \frac{f(\mathbf{z}_{a_{k,n}, n} | \underline{\mathbf{x}}_{k,n})}{f_{\text{fa}}(\mathbf{z}_{a_{k,n}, n})} \right) \\ & \times \left( \prod_{m \in \mathcal{N}_{\bar{\mathbf{r}}_n}} \frac{f(\mathbf{z}_{m,n} | \bar{\mathbf{x}}_{m,n})}{f_{\text{fa}}(\mathbf{z}_{m,n})} \right). \end{aligned} \quad (53)$$

Since the normalization factor  $C(\mathbf{z}_n) = \prod_{m=1}^{M_n} f_{\text{fa}}(\mathbf{z}_{m,n})$  depending on  $\mathbf{z}_n$  and  $M_n$  is fixed after the current measurement  $\mathbf{z}_n$  is observed, the likelihood function in (53) can be rewritten up to the normalization constant as

$$\begin{aligned} & f(\mathbf{z}_n | \underline{\mathbf{y}}_n, \bar{\mathbf{y}}_n, \mathbf{a}_n, \mathbf{b}_n, M_n) \\ & \propto \left( \prod_{k=1}^{K_{n-1}} g_2(\underline{\mathbf{y}}_{k,n}, a_{k,n}; \mathbf{z}_n) \right) \left( \prod_{m=1}^{M_n} h_2(\bar{\mathbf{y}}_{m,n}, b_{m,n}; \mathbf{z}_n) \right) \end{aligned} \quad (54)$$

where the factor related to legacy PMPC states  $g_2(\underline{\mathbf{y}}_{k,n}, a_{k,n}; \mathbf{z}_n) = g_2(\underline{\mathbf{x}}_{k,n}, \underline{\mathbf{r}}_{k,n}, a_{k,n}; \mathbf{z}_n)$  is given by

$$\begin{aligned} & g_2(\underline{\mathbf{x}}_{k,n}, \underline{\mathbf{r}}_{k,n} = 1, a_{k,n}; \mathbf{z}_n) \\ & \triangleq \begin{cases} \frac{f(\mathbf{z}_{m,n} | \underline{\mathbf{x}}_{k,n})}{f_{\text{fa}}(\mathbf{z}_{m,n})}, & a_{k,n} = m \\ 1, & a_{k,n} = 0 \end{cases} \end{aligned} \quad (55)$$

and  $g_2(\underline{\mathbf{x}}_{k,n}, \underline{\mathbf{r}}_{k,n} = 0, a_{k,n}; \mathbf{z}_n) \triangleq 1$ . The factor related to new PMPC states  $h_2(\bar{\mathbf{y}}_{m,n}, b_{m,n}; \mathbf{z}_n) = h_2(\bar{\mathbf{x}}_{m,n}, \bar{\mathbf{r}}_{m,n}, b_{m,n}; \mathbf{z}_n)$  is given by

$$\begin{aligned} & h_2(\bar{\mathbf{x}}_{m,n}, \bar{\mathbf{r}}_{m,n} = 1, b_{m,n}; \mathbf{z}_n) \\ & \triangleq \begin{cases} 1, & b_{m,n} = k \\ \frac{f(\mathbf{z}_{m,n} | \bar{\mathbf{x}}_{m,n})}{f_{\text{fa}}(\mathbf{z}_{m,n})}, & b_{m,n} = 0 \end{cases} \end{aligned} \quad (56)$$

and  $h_2(\bar{\mathbf{x}}_{m,n}, \bar{\mathbf{r}}_{m,n} = 0, b_{m,n}; \mathbf{z}_n) \triangleq 1$ . Inserting (54) (55) and (56) into (51), the conditional PDF can be rewritten as the joint likelihood function

$$\begin{aligned} & f(\mathbf{z}_{1:n} | \underline{\mathbf{y}}_{1:n}, \bar{\mathbf{y}}_{1:n}, \mathbf{a}_{1:n}, \mathbf{b}_{1:n}, \mathbf{m}_{1:n}) \\ & \propto \left( \prod_{m=1}^{M_1} h_2(\bar{\mathbf{x}}_{m,1}, \bar{\mathbf{r}}_{m,1}, b_{m,1}; \mathbf{z}_1) \right) \\ & \times \prod_{n'=2}^n \left( \prod_{k=1}^{K_{n'-1}} g_2(\underline{\mathbf{x}}_{k,n'}, \underline{\mathbf{r}}_{k,n'}, a_{k,n'}; \mathbf{z}_{n'}) \right) \\ & \times \left( \prod_{m'=1}^{M_{n'}} h_2(\bar{\mathbf{x}}_{m',n'}, \bar{\mathbf{r}}_{m',n'}, b_{m',n'}; \mathbf{z}_{n'}) \right). \end{aligned} \quad (57)$$

### C. Joint Posterior PDF

Finally, by substituting the joint prior PDF with (50) and the joint likelihood function with (57), the joint posterior PDF (10) can be rewritten as

$$\begin{aligned} & f(\mathbf{y}_{1:n}, \mathbf{a}_{1:n}, \mathbf{b}_{1:n}, \boldsymbol{\mu}_{\text{fa}1:n}, \mathbf{m}_{1:n} | \mathbf{z}_{1:n}) \\ & \propto f(\boldsymbol{\mu}_{\text{fa}1}) \left( \prod_{l=1}^{M_1} h_1(\bar{\mathbf{y}}_{l,1}, b_{l,1}, \mu_{\text{fa}1}; M_1) h_2(\bar{\mathbf{y}}_{l,1}, b_{l,1}; \mathbf{z}_1) \right) \\ & \times \prod_{n'=2}^n f(\boldsymbol{\mu}_{\text{fa}n'} | \boldsymbol{\mu}_{\text{fa}n'-1}) \left( \prod_{k'=1}^{K_{n'-1}} f(\underline{\mathbf{y}}_{k',n'} | \mathbf{y}_{k',n'-1}) \right) \\ & \times \left( \prod_{k=1}^{K_{n'-1}} g_1(\underline{\mathbf{y}}_{k,n'}, a_{k,n'}, \mu_{\text{fa}n'}; M_{n'}) g_2(\underline{\mathbf{y}}_{k,n'}, a_{k,n'}; \mathbf{z}_{n'}) \right) \\ & \times \prod_{m=1}^{M_{n'}} \psi(a_{k,n'}, b_{m,n'}) \left( \prod_{m'=1}^{M_{n'}} h_1(\bar{\mathbf{y}}_{m',n'}, b_{m',n'}, \mu_{\text{fa}n'}; M_{n'}) \right) \\ & \times h_2(\bar{\mathbf{y}}_{m',n'}, b_{m',n'}; \mathbf{z}_{n'}). \end{aligned} \quad (58)$$

The factors related to the legacy PMPCs and to the new PMPCs can be simplified as  $g(\underline{\mathbf{y}}_{k,n}, a_{k,n}, \mu_{\text{fa}n}; \mathbf{z}_n) \triangleq g_1(\underline{\mathbf{y}}_{k,n}, a_{k,n}, \mu_{\text{fa}n}; M_n) g_2(\underline{\mathbf{y}}_{k,n}, a_{k,n}; \mathbf{z}_n)$  and  $h(\bar{\mathbf{y}}_{m,n}, b_{m,n}, \mu_{\text{fa}n}; \mathbf{z}_n) \triangleq h_1(\bar{\mathbf{y}}_{m,n}, b_{m,n}, \mu_{\text{fa}n}; M_n) h_2(\bar{\mathbf{y}}_{m,n}, b_{m,n}; \mathbf{z}_n)$ , respectively (see Fig. 1).

### D. Squared Scale Parameter of the Truncated Rician PDF

Here, we derive the squared scale parameter of the truncated Rician PDF in (9) in Section III-C. We follow [45, Ch. 3.8] and approximate the squared scale parameter using the Fisher information which is sufficiently accurate for large amplitudes and large  $N_s H$ .<sup>6</sup> For simplicity, we assume that the MPCs

<sup>6</sup>Note that for unknown noise variance the distribution of the normalized amplitude measurement  $z_{u_{m,n}}$  is not described by a Rician distribution anymore. More specifically, the statistic of two times the squared PMPC-oriented normalized amplitude measurements  $2z_{u_{m,n}}^2$  is described by a non-central Fisher distribution [54], [55, Ch. 15.10.3]. For large  $N_s H$ , the statistic of  $2z_{u_{m,n}}^2$  can be well approximated by a non-central  $\chi^2$  distribution [44, Ch. 2.2] and therefore the statistic of the normalized amplitude measurement  $z_{u_{m,n}}$  by a Rician distribution. However, the proof and the details are out-of-scope of this paper.

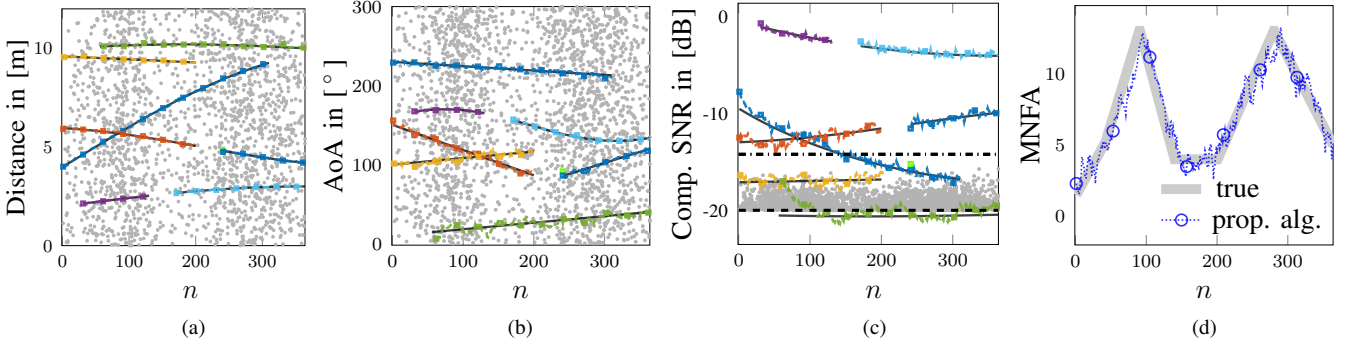


Fig. 8: Results of the proposed algorithm for fully synthetic measurements given  $\text{SNR}_{1m}^{\text{in}} = 5.4$  dB. The gray dots denote the false alarm measurements. The black solid lines denote the true MPC parameters. The estimates of different MPCs are denoted with densely-dashed lines with square markers in different colors. The horizontal dashed and dash-dotted lines in (c) indicate the thresholds of  $-20$  dB and  $-14.4$  dB respectively.

are well separated in dispersion space, so that their mutual correlations are negligible. We first determine the FIM for  $\boldsymbol{\xi}_{l,n} = [\Re\{\tilde{\alpha}_{l,n}\} \Im\{\tilde{\alpha}_{l,n}\} \sigma^2]^T$ , where  $\Re\{\tilde{\alpha}_{l,n}\}$  and  $\Im\{\tilde{\alpha}_{l,n}\}$  denote the real and imaginary parts of the complex amplitudes  $\tilde{\alpha}_{l,n}$ , and then apply the chain rule [45] to get the FIM for  $\tilde{u}_{l,n}$ . According to [45], the elements of the FIM for  $\tilde{\boldsymbol{\xi}}_{l,n}$  are given by

$$[\mathbf{J}_{l,n}(\boldsymbol{\xi}_{l,n})]_{i,j} = 2\Re \left\{ \frac{\partial \tilde{\alpha}_{l,n} \mathbf{s}^H(\tilde{\boldsymbol{\theta}}_{l,n}) \mathbf{C}^{-1} \frac{\partial \mathbf{s}(\tilde{\boldsymbol{\theta}}_{l,n}) \tilde{\alpha}_{l,n}}{\partial [\xi_{l,n}]_j}}{\partial [\xi_{l,n}]_i} \right\} + \text{tr} \left\{ \mathbf{C}^{-1} \frac{\partial \mathbf{C}^{-1}}{\partial [\xi_{l,n}]_i} \mathbf{C}^{-1} \frac{\partial \mathbf{C}^{-1}}{\partial [\xi_{l,n}]_j} \right\} \quad (59)$$

where  $i, j \in \{1, 2, 3\}$ . After some straightforward calculations (59) can be rewritten as

$$\mathbf{J}_{l,n}(\boldsymbol{\xi}_{l,n}) = \text{diag} \left\{ \frac{2\|\mathbf{s}(\tilde{\boldsymbol{\theta}}_{l,n})\|^2}{\sigma^2}, \frac{2\|\mathbf{s}(\tilde{\boldsymbol{\theta}}_{l,n})\|^2}{\sigma^2}, \frac{N_s H}{\sigma^4} \right\}. \quad (60)$$

The CRLB for  $\tilde{u}_{l,n}$  is obtained by applying the chain rule, i.e.,

$$\sigma_{\tilde{u}_{l,n}}^2 \triangleq J_{\tilde{u}_{l,n}}^{-1}(\tilde{u}_{l,n}) = \mathbf{t}_{l,n}^H \mathbf{J}_{l,n}^{-1}(\boldsymbol{\xi}_{l,n}) \mathbf{t}_{l,n} = \frac{1}{2} + \frac{\tilde{u}_{l,n}^2}{4N_s H} \quad (61)$$

where the Jacobian  $\mathbf{t}_{l,n}$  containing the partial derivatives is

$$\mathbf{t}_{l,n} \triangleq \begin{bmatrix} \frac{\partial \tilde{u}_{l,n}}{\partial \Re\{\tilde{\alpha}_{l,n}\}} & \frac{\partial \tilde{u}_{l,n}}{\partial \Im\{\tilde{\alpha}_{l,n}\}} & \frac{\partial \tilde{u}_{l,n}}{\partial \sigma^2} \end{bmatrix}^T = \begin{bmatrix} \frac{\Re\{\tilde{\alpha}_{l,n}\} \|\mathbf{s}(\tilde{\boldsymbol{\theta}}_{l,n})\|}{|\tilde{\alpha}_{l,n}| \sigma} & \frac{\Im\{\tilde{\alpha}_{l,n}\} \|\mathbf{s}(\tilde{\boldsymbol{\theta}}_{l,n})\|}{|\tilde{\alpha}_{l,n}| \sigma} & \frac{-|\tilde{\alpha}_{l,n}| \|\mathbf{s}(\tilde{\boldsymbol{\theta}}_{l,n})\|}{2\sigma^3} \end{bmatrix}^T. \quad (62)$$

Note that the second term  $\frac{\tilde{u}_{l,n}^2}{4N_s H}$  in (61) characterizes the effect of the noise variance estimation, which becomes significant for high component SNRs, and converges to zero for low component SNRs or a large  $N_s H$ . Thus, for PMPC-oriented

measurements the squared scale parameter of the truncated Rician PDF in (9) is given by (61) and for false alarm measurements the squared scale parameter of the Rayleigh PDF is given by  $1/2$ .

### E. Additional Simulation Results

1) *Fast Varying MNFA*: As shown in Section VII-B1, the proposed algorithm accurately estimate the slow varying MNFA. With an increased standard deviation of the driving noise to the MNFA state-transition PDF  $\sigma_{\text{fa}} = 0.5$ , the results for fully synthetic measurements shown in Fig. 8 further demonstrate the excellent performance of the proposed algorithm when handling fast varying MNFA.

2) *Synthetic Radio Measurements*: Fig. 9 presents the results of the proposed algorithm and the KEST algorithm of an exemplary simulation run given  $\text{SNR}_{1m}^{\text{in}} = 5.4$  dB. When handling well-separated MPCs with high component SNRs, the algorithms perform similarly good. The slightly over estimated component SNRs shown in Fig. 9c are due to the Gaussian approximation on the likelihood function (see for Section VII-A1). Regarding the MPC below the threshold of  $-18$  dB, it is immediately detected and accurately estimated in the proposed algorithm but totally missed in the KEST algorithm. Additionally, with probabilistic DA the proposed algorithm properly copes with intersecting MPCs around  $n = 83$ , while the association uncertainty which further leads to discontinuity of sequential estimations is clearly shown with the KEST algorithm.

3) *Runtime Analysis*: The overall computational complexity of a sequential channel estimation method depends on many factors like the NoM and the number of measurements, and mostly importantly the complexity of snapshot-based channel estimator. Fig. 10a depicts the mean runtimes per time step of the proposed algorithm and the KEST algorithm for synthetic radio measurements.<sup>7</sup> The mean runtimes are obtained by averaging over all simulation runs and time steps for

<sup>7</sup>The simulation results were obtained by running MATLAB implementations on a cluster of computers with different hardware configurations.

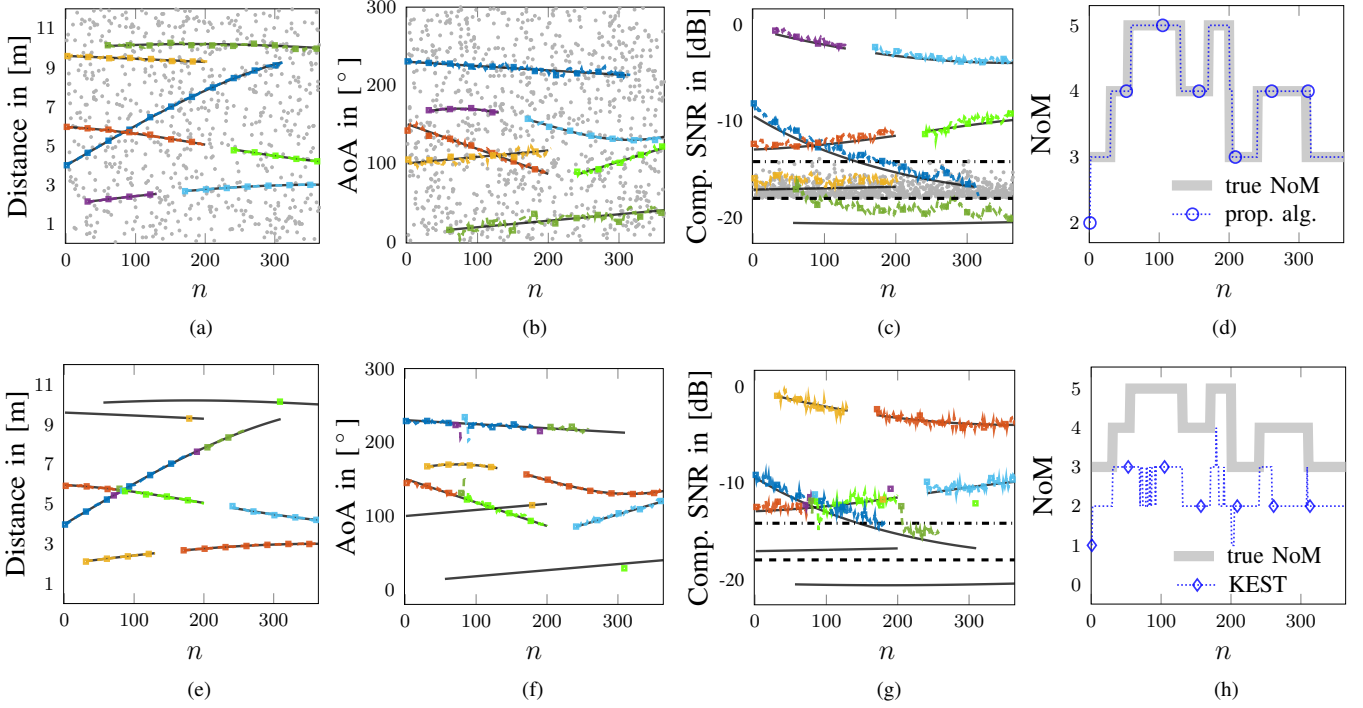


Fig. 9: Results for synthetic radio measurements given  $\text{SNR}_{1m}^{\text{in}} = 5.4\text{ dB}$ : (a) to (d), results of the proposed algorithm, the gray dots denote the false alarm measurements. (e) to (h), results of the KEST algorithm. The black solid lines denote the true MPC parameters. The estimates of different MPCs are denoted with densely-dashed lines with square markers in different colors. The horizontal dashed and dash-dotted lines indicate the thresholds of  $-18\text{ dB}$  and  $-14.4\text{ dB}$  respectively.

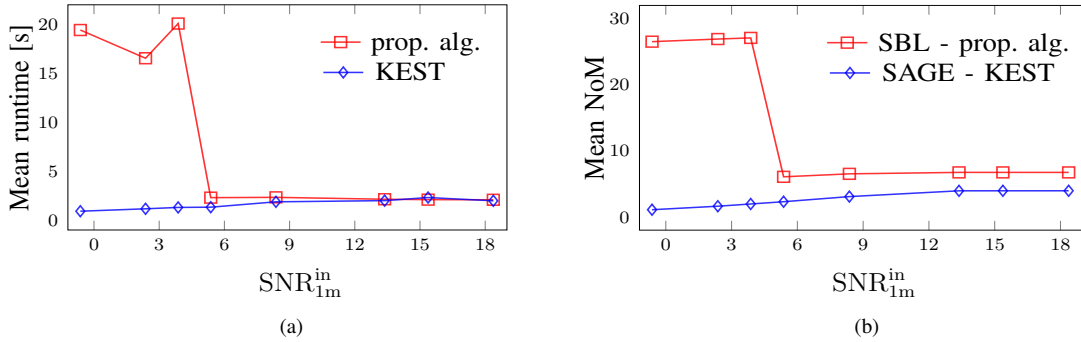


Fig. 10: Mean runtimes per time step of the proposed algorithm and the KEST algorithm using MATLAB implementations, and the mean NoM per time step estimated using the snapshot-based channel estimators SBL and SAGE for synthetic radio measurements. The mean values are obtained by averaging over all simulation runs and time steps for each  $\text{SNR}_{1m}^{\text{in}} \in \{-0.6, 2.4, 3.9, 5.4, 8.4, 13.4, 15.4, 18.4\}\text{ dB}$ .

each  $\text{SNR}_{1m}^{\text{in}} \in \{-0.6, 2.4, 3.9, 5.4, 8.4, 13.4, 15.4, 18.4\}\text{ dB}$ . When the  $\text{SNR}_{1m}^{\text{in}}$  is larger than 5 dB, the mean NoMs estimated in the SBL and the SAGE parametric channel estimators are comparable as shown in Fig. 10b,<sup>8</sup> and the mean runtimes of the proposed algorithm and the KEST algorithm are both approximately 2 s/step as depicted in Fig. 10a. For  $\text{SNR}_{1m}^{\text{in}}$  smaller than 5 dB the detection threshold  $u_{\text{de}}^{\text{in}}$  in the SBL channel estimator is further relaxed from  $-18\text{ dB}$  to  $-20\text{ dB}$  to support the detection of low SNR MPCs (see for Sec-

<sup>8</sup>At each time step, the KEST algorithm needs to run the SAGE channel estimator several times for testing different NoM hypotheses, the mean NoM of the SAGE shown in Fig. 10b depicts the mean NoM chosen by the MDL principle used in the KEST.

tion VII-B2), therefore the mean NoM per time step estimated in the SBL increased sharply from 5 to 30, correspondingly the mean runtime increased from 2 s/step to 20 s/step. The results above illustrate that the mean runtime is approximately linear-proportional to the mean NoM estimated in the snapshot-based channel estimator.

## REFERENCES

- [1] M. L. Jakobsen, T. Pedersen, and B. H. Fleury, "Analysis of stochastic radio channels with temporal birth-death dynamics: A marked spatial point process perspective," *IEEE Trans. Antennas Propag.*, vol. 62, no. 7, pp. 3761–3775, Apr. 2014.
- [2] J. Flordelis, X. Li, O. Edfors, and F. Tufvesson, "Massive MIMO extensions to the COST 2100 channel model: Modeling and validation," *IEEE Trans. Wireless Commun.*, vol. 19, no. 1, pp. 380–394, Oct. 2020.

- [3] F. Rusek, D. Persson, B. K. Lau, E. G. Larsson, T. L. Marzetta, O. Edfors, and F. Tufvesson, "Scaling up MIMO: Opportunities and challenges with very large arrays," *IEEE Signal Process. Mag.*, vol. 30, no. 1, pp. 40–60, Jan. 2013.
- [4] R. Di Taranto, S. Muppirisetty, R. Raulefs, D. Slock, T. Svensson, and H. Wymeersch, "Location-aware communications for 5G networks: How location information can improve scalability, latency, and robustness of 5G," *IEEE Signal Process. Mag.*, vol. 31, no. 6, pp. 102–112, Nov. 2014.
- [5] S. Hu, F. Rusek, and O. Edfors, "Beyond massive MIMO: The potential of data transmission with large intelligent surfaces," *IEEE Trans. Signal Process.*, vol. 66, no. 10, pp. 2746–2758, May 2018.
- [6] C. Gentner, T. Jost, W. Wang, S. Zhang, A. Dammann, and U. C. Fiebig, "Multipath assisted positioning with simultaneous localization and mapping," *IEEE Trans. Wireless Commun.*, vol. 15, no. 9, pp. 6104–6117, Sept. 2016.
- [7] E. Leitinger, F. Meyer, F. Tufvesson, and K. Witrisal, "Factor graph based simultaneous localization and mapping using multipath channel information," in *Proc. IEEE ICCW-17*, Paris, France, May 2017, pp. 652–658.
- [8] E. Leitinger, F. Meyer, F. Hlawatsch, K. Witrisal, F. Tufvesson, and M. Z. Win, "A belief propagation algorithm for multipath-based SLAM," *IEEE Trans. Wireless Commun.*, vol. 18, no. 12, pp. 5613–5629, Dec. 2019.
- [9] R. Mendrzik, F. Meyer, G. Bauch, and M. Z. Win, "Enabling situational awareness in millimeter wave massive MIMO systems," *IEEE J. Sel. Topics Signal Process.*, vol. 13, no. 5, pp. 1196–1211, Sept. 2019.
- [10] E. Leitinger and F. Meyer, "Data fusion for multipath-based SLAM," in *Proc. Asilomar-20*, Pacific Grove, CA, USA, Oct. 2020, pp. 934–939.
- [11] S. Grebien, E. Leitinger, K. Witrisal, and B. H. Fleury, "Super-resolution channel estimation including the dense multipath component — A sparse Bayesian approach," 2021, in preperation.
- [12] R. Schmidt, "Multiple emitter location and signal parameter estimation," *IEEE Trans. Antennas Propag.*, vol. 34, no. 3, pp. 276–280, Mar. 1986.
- [13] R. Roy and T. Kailath, "ESPRIT-estimation of signal parameters via rotational invariance techniques," *IEEE Trans. Acoust., Speech, Signal Process.*, vol. 37, no. 7, pp. 984–995, Jul. 1989.
- [14] M. Haardt, F. Roemer, and G. Del Galdo, "Higher-order SVD-based subspace estimation to improve the parameter estimation accuracy in multidimensional harmonic retrieval problems," *IEEE Trans. Signal Process.*, vol. 56, no. 7, pp. 3198–3213, Jun. 2008.
- [15] B. Ottersten, M. Viberg, P. Stoica, and A. Nehorai, "Exact and large sample maximum likelihood techniques for parameter estimation and detection in array processing," in *Radar Array Processing*. Springer, 1993, pp. 99–151.
- [16] J. A. Fessler and A. O. Hero, "Space-alternating generalized expectation-maximization algorithm," *IEEE Trans. Signal Process.*, vol. 42, no. 10, pp. 2664–2677, Oct. 1994.
- [17] B. H. Fleury, M. Tschudin, R. Heddergott, D. Dahlhaus, and K. Ingeman Pedersen, "Channel parameter estimation in mobile radio environments using the SAGE algorithm," *IEEE J. Sel. Areas Commun.*, vol. 17, no. 3, pp. 434–450, 1999.
- [18] A. Richter, "Estimation of radio channel parameters: Models and algorithms," Ph.D. dissertation, Ilmenau University of Technology, 2005.
- [19] P. Stoica and Y. Selen, "Model-order selection: A review of information criterion rules," *IEEE Signal Process. Mag.*, vol. 21, no. 4, pp. 36–47, Jul. 2004.
- [20] D. Shutin and B. H. Fleury, "Sparse variational Bayesian SAGE algorithm with application to the estimation of multipath wireless channels," *IEEE Trans. Signal Process.*, vol. 59, no. 8, pp. 3609–3623, Aug. 2011.
- [21] M. A. Badiu, T. L. Hansen, and B. H. Fleury, "Variational Bayesian inference of line spectra," *IEEE Trans. Signal Process.*, vol. 65, no. 9, pp. 2247–2261, May 2017.
- [22] T. L. Hansen, B. H. Fleury, and B. D. Rao, "Superfast line spectral estimation," *IEEE Trans. Signal Process.*, vol. PP, no. 99, pp. 1–1, 2018.
- [23] J. Salmi, A. Richter, and V. Koivunen, "Detection and tracking of MIMO propagation path parameters using state-space approach," *IEEE Trans. Signal Process.*, vol. 57, no. 4, pp. 1538–1550, Apr. 2009.
- [24] X. Li, E. Leitinger, M. Oskarsson, K. Åström, and F. Tufvesson, "Massive MIMO-based localization and mapping exploiting phase information of multipath components," *IEEE Trans. Wireless Commun.*, vol. 18, no. 9, pp. 4254–4267, Sept. 2019.
- [25] D. Shutin and B. Vexler, "Sparse Bayesian learning with dictionary refinement for super-resolution through time," in *Proc. IEEE CAMSAP-17*, Dec. 2017, pp. 1–5.
- [26] F. Meyer, Y. Park, and P. Gerstoft, "Variational Bayesian estimation of time-varying DOAs," in *Proc. IEEE Fusion-20*, Rustenburg, South Africa, Sept. 2020, pp. 1–6.
- [27] T. Jost, W. Wang, U. Fiebig, and F. Perez-Fontan, "Detection and tracking of mobile propagation channel paths," *IEEE Trans. Antennas Propag.*, vol. 60, no. 10, pp. 4875–4883, Oct. 2012.
- [28] Y. Bar-Shalom, P. K. Willett, and X. Tian, *Tracking and data fusion: A handbook of algorithms*. Storrs, CT, USA: Yaakov Bar-Shalom, 2011.
- [29] F. Meyer, T. Kropfreiter, J. L. Williams, R. Lau, F. Hlawatsch, P. Braca, and M. Z. Win, "Message passing algorithms for scalable multitarget tracking," *Proc. IEEE*, vol. 106, no. 2, pp. 221–259, Feb. 2018.
- [30] D. Shutin, W. Wang, and T. Jost, "Incremental sparse Bayesian learning for parameter estimation of superimposed signals," in *Proc. SAMPTA-2013*, no. 1, Sept. 2013, pp. 6–9.
- [31] E. Leitinger, S. Grebien, X. Li, F. Tufvesson, and K. Witrisal, "On the use of MPC amplitude information in radio signal based SLAM," in *Proc. IEEE SSP-18*, Freiburg, Germany, Jun. 2018, pp. 633–637.
- [32] E. Leitinger, S. Grebien, and K. Witrisal, "Multipath-based SLAM exploiting AoA and amplitude information," in *Proc. IEEE ICCW-19*, Shanghai, China, May 2019, pp. 1–7.
- [33] F. Meyer and J. L. Williams, "Scalable detection and tracking of geometric extended objects," *IEEE Trans. Signal Process.*, vol. 69, pp. 6283–6298, Oct. 2021.
- [34] F. Meyer and K. L. Gemba, "Probabilistic focalization for shallow water localization," *J. Acoust. Soc. Am.*, 2021.
- [35] F. Meyer, P. Braca, P. Willett, and F. Hlawatsch, "A scalable algorithm for tracking an unknown number of targets using multiple sensors," *IEEE Trans. Signal Process.*, vol. 65, no. 13, pp. 3478–3493, Jul. 2017.
- [36] D. Lerro and Y. Bar-Shalom, "Automated tracking with target amplitude information," in *1990 American Control Conf.*, May 1990, pp. 2875–2880.
- [37] G. Soldi, F. Meyer, P. Braca, and F. Hlawatsch, "Self-tuning algorithms for multisensor-multitarget tracking using belief propagation," *IEEE Trans. Signal Process.*, vol. 67, no. 15, pp. 3922–3937, Aug. 2019.
- [38] X. Li, E. Leitinger, and F. Tufvesson, "Detection and tracking of multipath channel parameters using belief propagation," in *Proc. Asilomar-20*, Pacific Grove, CA, USA, Nov. 2020, pp. 1083–1089.
- [39] E. Leitinger, S. Grebien, B. H. Fleury, and K. Witrisal, "Detection and estimation of a spectral line in MIMO systems," in *Proc. Asilomar-20*, Pacific Grove, CA, USA, Nov. 2020, pp. 1090–1095.
- [40] T. Wilding, S. Grebien, E. Leitinger, U. Mühlmann, and K. Witrisal, "Single-anchor, multipath-assisted indoor positioning with aliased antenna arrays," in *Asilomar-18*, Pacific Grove, CA, USA, Oct. 2018, pp. 525–531.
- [41] J. Williams and R. Lau, "Approximate evaluation of marginal association probabilities with belief propagation," *IEEE Trans. Aerosp. Electron. Syst.*, vol. 50, no. 4, pp. 2942–2959, Oct. 2014.
- [42] F. Kschischang, B. Frey, and H.-A. Loeliger, "Factor graphs and the sum-product algorithm," *IEEE Trans. Inf. Theory*, vol. 47, no. 2, pp. 498–519, Feb. 2001.
- [43] H.-A. Loeliger, "An introduction to factor graphs," *IEEE Signal Process. Mag.*, vol. 21, no. 1, pp. 28–41, Feb. 2004.
- [44] S. Kay, *Fundamentals of Statistical Signal Processing: Detection Theory*. Upper Saddle River, NJ, USA: Prentice-H, 1998.
- [45] S. Kay, *Fundamentals of Statistical Signal Processing: Estimation Theory*. Upper Saddle River, NJ, USA: Prentice-H, 1993.
- [46] F. Meyer, O. Hlinka, H. Wymeersch, E. Riegler, and F. Hlawatsch, "Distributed localization and tracking of mobile networks including noncooperative objects," *IEEE Trans. Signal Inf. Process. Net.*, vol. 2, no. 1, pp. 57–71, Mar. 2016.
- [47] P. Tichavsky, C. Muravchik, and A. Nehorai, "Posterior Cramer-Rao bounds for discrete-time nonlinear filtering," *IEEE Trans. Signal Process.*, vol. 46, no. 5, pp. 1386–1396, May 1998.
- [48] Y. Bar-Shalom, T. Kirubarajan, and X.-R. Li, *Estimation with Applications to Tracking and Navigation*. New York, NY, USA: Wiley, 2002.
- [49] D. Schuhmacher, B.-T. Vo, and B.-N. Vo, "A consistent metric for performance evaluation of multi-object filters," *IEEE Trans. Signal Process.*, vol. 56, no. 8, pp. 3447–3457, Aug. 2008.
- [50] P. Meissner, E. Leitinger, M. Lafer, and K. Witrisal, "MeasureMINT UWB database," 2013. [Online]. Available: [www.spssc.tugraz.at/tools/UWBmeasurements](http://www.spssc.tugraz.at/tools/UWBmeasurements)
- [51] E. Leitinger, P. Meissner, C. Rüdiger, G. Dumphart, and K. Witrisal, "Evaluation of position-related information in multipath components for

indoor positioning,” *IEEE J. Sel. Areas Commun.*, vol. 33, no. 11, pp. 2313–2328, Nov. 2015.

- [52] A. Venus, E. Leitinger, S. Tertinek, and K. Witrissal, “A message passing based adaptive PDA algorithm for robust radio-based localization and tracking,” in *IEEE RadarConf21*, May 2021, pp. 1–6.
- [53] M. Beard, B.-T. Vo, and B.-N. Vo, “Bayesian multi-target tracking with merged measurements using labelled random finite sets,” *IEEE Trans. Signal Process.*, vol. 63, no. 6, pp. 1433–1447, Jan. 2015.
- [54] K. J. Worsley, “Local maxima and the expected euler characteristic of excursion sets of  $\chi^2$ ,  $f$  and  $t$  fields,” *Adv. Appl. Probab.*, vol. 26, no. 1, pp. 13–42, 1994. [Online]. Available: <http://www.jstor.org/stable/1427576>
- [55] R. J. Adler and J. E. Taylor, *Random Fields and Geometry*. New York, NY, USA: Springer, 2007.



**Fredrik Tufvesson** received his Ph.D. in 2000 from Lund University in Sweden. After two years at a startup company, he joined the department of Electrical and Information Technology at Lund University, where he is now professor of radio systems. His main research interest is the interplay between the radio channel and the rest of the communication system with various applications in 5G/B5G systems such as massive MIMO, mm wave communication, vehicular communication and radio based positioning.

Fredrik has authored around 100 journal papers and 150 conference papers, he is fellow of the IEEE and his research has been awarded with the Neal Shepherd Memorial Award (2015) for the best propagation paper in IEEE TRANSACTIONS ON VEHICULAR TECHNOLOGY and the IEEE COMMUNICATIONS SOCIETY best tutorial paper award (2018, 2021).



**Xuhong Li** received her B.Sc. degree in telecommunication engineering from Jilin University, China, in 2010, and her M.Sc. degree in wireless communication from Lund University, Lund, Sweden, in 2014. Currently, she is pursuing her Ph.D. degree at the Department of Electrical and Information Technology, Lund University. Her research interests include radio-based localization and estimation of radio channels.



**Erik Leitinger** (Member, IEEE) received the Dipl.-Ing. (M.Sc.) and Ph.D. degrees (with highest Hons.) in electrical engineering from Graz University of Technology, Austria in 2012 and 2016. He is currently Senior Research Scientist with the Graz University of Technology. From 2016 to 2018, he was Postdoctoral Researcher at the department of Electrical and Information Technology at Lund University. He is an Erwin Schrödinger Fellow.

Dr. Leitinger received an Award of Excellence from the Federal Ministry of Science, Research and Economy (BMWF) for his Ph.D. Thesis. He served as co-chair of the special session “Synergistic Radar Signal Processing and Tracking” at the IEEE Radar Conference in 2021 and co-organizer of the special issue “Graph-Based Localization and Tracking” in the Journal of Advances in Information Fusion (JAIF). His research interests include statistical signal processing, nonlinear estimation and detection, inference on graphs, localization and navigation, SLAM, estimation of radio channels, and estimation/detection theory.



**Alexander Venus** (S’20) received his B.Sc. and Dipl.-Ing. (M.Sc.) degrees (with highest Hons.) in biomedical engineering and information and communication engineering from Graz University of Technology, Austria in 2012 and 2015, respectively. He was a research and development engineer at Anton Paar GmbH, Graz from 2014 to 2019. He is currently a project assistant at Graz University of Technology, where he is pursuing his Ph.D. degree.

His research interests include radio-based localization and navigation, estimation of radio channels, inference on graphs, stochastic modeling, and estimation/detection theory.